Stress analysis of single-bolt, single-lap, countersunk composite joints with variable bolt-hole clearance

Brian Egan, Conor Mc Carthy, Michael McCarthy, Ronan Frizzell

Stress Analysis of Single-Bolt, Single-Lap, Countersunk Composite Joints with Variable Bolt-Hole Clearance

B. Egan, C.T. McCarthy, M.A. McCarthy, R.F. Frizzell

PII: S0263-8223(11)00367-9
DOI: 10.1016/j.compstruct.2011.10.004
Reference: COST 4407

To appear in: *Composite Structures*

Please cite this article as: Egan, B., McCarthy, C.T., McCarthy, M.A., Frizzell, R.F., Stress Analysis of Single-Bolt, Single-Lap, Countersunk Composite Joints with Variable Bolt-Hole Clearance, *Composite Structures* (2011), doi: 10.1016/j.compstruct.2011.10.004

Authors: B. Egan, C.T. McCarthy*, M.A. McCarthy, R.F. Frizzell

Affiliation: *Materials and Surface Science Institute (MSSI) and the Department of Mechanical, Aeronautical and Biomedical Engineering, University of Limerick, Ireland*

Abstract

Single-lap, carbon-epoxy joints with countersunk fasteners were modelled using the non-linear finite element code Abaqus. A highly-detailed analysis of the stress distribution at the countersunk hole boundary is provided. Bolt-hole clearance, which arises due to limitations in manufacturing capabilities, is modelled extensively. Clearance levels both inside and outside typical aerospace fitting tolerances are studied and the finite element model is validated with experimental data. Plots of radial stress in each ply of the countersunk laminate show the load transfer to be severely localised, with only a few plies bearing the majority of the load. The inclusion of clearance in the model was shown result in far higher radial stresses compared to those in the neat-fit joint model. An associated loss in joint stiffness of more than 10% was recorded for the highest clearance considered (240 μm). Finally compressive through-thickness stresses are shown to be present at the damageable region of the countersunk hole, and increase with bolt-hole clearance. These compressive stresses, which are an indicator of lateral constraint, are seen to suppress "brooming" failure in the countersunk laminate.

Keywords

Finite Element Analysis, Carbon-epoxy, Clearance, Bolted Joints, Countersunk, Bearing Failure

* Corresponding Author: Tel.: +353-61-234334; fax: +353-61-202944

Email address: conor.mccarthy@ul.ie (C.T. McCarthy)

1 Introduction

The inclusion of bolted joints in aircraft structures leads to regions of stress concentration. Composite materials are relatively brittle and typically offer limited stress relief through localised yielding compared to metals. This, combined with inadequate failure prediction capabilities, can lead to conservatively designed composite bolted joints which amount to severe structural weight penalties [1]. Bonded joints offer higher structural efficiency, but limit accessibility and can increase manufacturing and maintenance costs [2]. Optimising composite bolted joints using improved modelling tools thus continues to be a priority for airframe manufacturers. Countersunk fasteners are of particular interest for use in skin-structure joints where aerodynamic efficiency is important. Many of these joints are single-lap in nature. Single-lap joints result in significant stress concentrations and lower bearing strengths compared to double-lap joints [3-5], while countersunk joints clearly involve a highly complex stress distribution in the laminates. Thus countersunk, single-lap joints are of critical importance to the aircraft industry, but are also the most complex type to analyse. To date, there have been few detailed studies on this type of joint.

Ireman [6] developed three-dimensional (3D) finite element (FE) models of single-lap, single-bolt composite joints. Both protruding and countersunk-head fasteners, having neat-fit clearances, were modelled and results were compared to experimental tests. The FE strains exhibited good correlation with experimental strain gauge results. Secondary bending was greater in experiments than in the FE models, which was attributed to the use of overly-stiff linear elements. Contact pressure plots were extracted at the hole boundary and it was shown that for countersunk laminates, the bearing load was predominantly carried by the cylindrical part of the hole. These plots represented average contact pressures at nodes of the contact surfaces and variations in pressure due to ply orientations were excluded. Hühne et al. [7] carried out FE modelling on a single-lap composite joint incorporating a single countersunk rivet and liquid shim layer. Extensive investigations were necessary to determine a convergent contact formulation. Progressive damage modelling was used to successfully predict joint failure, but hole boundary stress distributions were not provided. A bolt pre-stress was included only to initiate contact between the laminates, and bolt-hole clearance was omitted.

In mechanical joining, manufacturing processes allow for a statistical distribution in the diameter of fasteners and holes, giving rise to variable bolt-hole clearance. Bolted composite joint tolerances provide for a neat-fit or a clearance-fit, with interference fits being generally avoided [8]. Several studies have been carried out on the effect of clearance in composite joints, but none have involved countersunk fasteners. Naik and Crews [9] carried out a two-dimensional (2D) FE analysis on a pin-loaded, carbon-epoxy joint with variable clearance. Increasing clearance, gave an increase in the local stresses and hole deformation. DiNicola and Fantle [8] carried out pin-loaded experiments and 2D FE modelling on carbon-epoxy laminates in double-shear. Clearances ranged from neat-fit to

279 μm, and a clearance of 150 μm was considered a limit for aerospace primary structures. Bearing strength,

defined by 4% hole deformation, was found to decrease with hole oversize. Kelly and Hallström [10] carried out an experimental and 3D FE study into the effect of clearance on the bearing strength of carbon-fibre reinforced plastic (CFRP) laminates made from non-crimp fabric. Clearance was again found to reduce joint stiffness and bearing strength. The model was used to investigate hole boundary stresses, and the magnitude of radial and through-thickness stresses at the hole boundary were found to increase significantly with clearance. Tensile through-thickness stresses were attributed to through-thickness laminate expansion due to the Poisson effect. Naik and Crews [9], Di Nicola and Fantle [8] and Kelly and Hallström [10] all demonstrated a reduced contact arc for increased clearance. The higher radial stresses at clearance-fit holes, and resulting stiffness loss, were attributed to the reduced contact area.

McCarthy et al. [11] conducted an experimental investigation into the effect of clearance on the stiffness and strength of single-bolt, single-lap, carbon-epoxy joints. The joints were sized to induce a bearing mode of failure, and were secured with both protruding and countersunk-head fasteners. Finger-tight and fully-torqued joints were tested, with

a finger-tightened bolt representing a worst case (loosened-bolt) scenario. Clearances ranged from neat-fit to 240μm or 3% of the 8mm bolt diameter. Countersunk joints failed initially in bearing at significantly lower loads than the protruding-head joints. The load-deflection curves of countersunk joints typically included a distinct 'knee', in contrast to the protruding-head joints. Increasing clearance was found to reduce joint stiffness for all joint configurations. The offset bearing strength of finger-tight, protruding-head joints decreased with clearance, but no such relationship was found for finger-tight countersunk joints. McCarthy et al. [12, 13] carried out a 3D FE study on single-lap, single-bolt, protruding-head joints. Results were compared with surface strains and joint stiffness measurements from McCarthy et al. [11]. Surface strains correlated well, but the predicted joint stiffness was high compared to the experimental stiffness, which was measured using extensometers and LVDT transducers. Refinements were then made to the model to provide better stiffness correlation. Stresses around the hole were compared with another highly-detailed (1.2 million degree of freedom (DOF), 4th order element) model, and showed good correlation, considering the relative coarseness of the unrefined model (20,000 DOF). Radial and tangential stresses in individual plies (extracted at the hole boundary) were shown to be highly non-uniform through the laminate thickness. For increased bolt-hole clearance, radial and tangential stress values were shown to localise, with peak values growing substantially. Reductions in the model stiffness for clearance-fit conditions compared well with experimental results.

Several studies have investigated the effect of lateral constraint on the strength of composite bolted joints. Stockdale and Matthews [14] carried out an experimental study on the effect of clamping pressure on bearing failure loads in glass-fibre reinforced plastics (GFRP). Tests were performed both under pin-loading and with washers and a bolt. A 40% increase on the pin-loaded bearing strength was achieved for the finger tight case, while a 100% increase was observed for maximum clamping load (14.7 kN). Bearing failure in the pin-loaded tests was shown to be a mixture of compressive damage and delamination failure. Collings [15] and Eriksson [16] found that bearing failure in unconstrained carbon-epoxy joints occurred through a similar buckling mode involving lateral "brooming" of the outer plies. Further studies on carbon-epoxy laminates with variable lateral constraint were carried out by Sun et al. [17], Park [18] and Kelly and Hallström [10]. Increased offset strengths of clamped specimens, compared to unconstrained specimens, were attributed to the fact that lateral clamping pressure suppresses the onset and propagation of delamination. Stockdale and Matthews [14] had previously shown that when restraining washers are included, delamination was prevented, even for the finger-tight condition. Kelly and Hallström [10] found that with lateral constraint, brooming failure was suppressed at the hole boundary and the through-thickness expansion moved to the washer edge, supporting observations of Stockdale and Matthews [14], Eriksson et al. [16] and Park [18]. Through FE modelling of pin-loaded laminates, Kelly and Hallström [10] demonstrated significant tensile through-thickness stress at the hole boundary, which was said to promote intralaminar and interlaminar fracture of the plies. Nassar et al. [19] investigated experimentally the effect of bolt-torque in single-lap, woven glass/epoxy composite joints (protruding head bolts). Finger-tight and fully-torqued conditions were examined. A microscopy study

following final rupture showed that no significant delamination occurred at holes of fully-torqued bolts, whereas delamination *was* observed at holes of finger-tight bolts.

From the above, it can be seen that studies on countersunk-bolt composite joints are few in number. Countersunk fasteners pose a difficult contact problem, which few have attempted, and the 3D layer-by-layer stress distribution developed at a countersunk hole boundary has not been reported in the literature. In addition, the effect of clearance on countersunk joints has been ignored except for the experimental study by McCarthy et al. [11]. The lateral constraint supplied by a countersunk bolt-washer-nut system has also not been studied. In the current paper, three-dimensional FE modelling is carried out on single-lap, single-bolt, countersunk composite joints of variable bolt-hole clearance, and results are compared to the experimental data of McCarthy et al. [11]. Layer-by-layer stress distributions are provided to give a clear insight into the mechanical behaviour of countersunk composite joints.

2 Problem Description

The current model parameters were chosen to match the experimental study of McCarthy et al. [11]. The joint dimensions are shown in Figure 1, and give geometric ratios designed to induce bearing failure (i.e. w/d = 6, d/t = 1.6, e/d = 3). The laminate material was pre-impregnated HTA/6376 carbon-epoxy, with the lay-up consisting of 40 plies in a quasi-isotropic (QI) stacking sequence $[45/0/-45/90]_{5s}$.

The 100° countersunk-head fasteners were made of an aerospace grade titanium alloy (Ti-6Al-4V) and secured with a steel nut and washer. As shown in Figure 2, the angled head of the bolt extends through a significant portion of the top laminate in the joint. A countersink cut depth of 3.4 mm, which corresponds to the depth of the angled head, results in a cylindrical thickness of 1.8 mm (denoted t_{cyl} in Figure 2). This is approximately the minimum t_{cyl} value allowed in airframe design [20]. Specifications in the MIL-HDBK-17 [4] allow the countersink to penetrate a maximum depth equal to 70% of the sheet thickness, with the depth here being 65.4%. However, the depth of the countersink cut realised in the experiments was based on fitting the fastener head snugly in the hole, resulting in tcyl values being slightly different to those nominally-specified. The t_{cyl} values used for the FE models were measured directly from micrographs of failed specimens (Lawlor [21]), and are provided in Table 1. The reason for the slight increase in t_{cyl} for the larger clearance holes is illustrated in Figure 2 (b).

The definition chosen here for fibre orientation (α) and contact angle (θ) (see Camanho and Matthews [22]) are shown in Figure 3 (a), and will be used for presenting plots of hole boundary stresses. A polar coordinate system, centred in the hole, and denoting radial (r), tangential (t) and through-thickness (z) directions allows for meaningful interpretation of stresses (see Figure 3 (b)).

The four clearances used in the experimental study, designated C1 to C4, are shown in Table 1. Nominal clearances range from 0 μm (neat fit) to 240 μm, but the tolerance on reamer and bolt diameters resulted in a range of possible values, as shown. For this bolt diameter (8 mm), the f7/H10 ISO fitting tolerance, which has been used in the aerospace industry, permits a maximum hole oversize of 86 μm (1.1% of 8 mm). The C3 and C4 values (2% and 3% clearance respectively) are of interest for investigating out-of-tolerance aerospace fittings. The pre-loads induced by the applied torque were determined in a separate study [23]. A finger-tight torque of 0.5 Nm induced a 7.2 MPa pre-stress in shanks of protruding-head bolts, and a similar value was anticipated for countersunk fasteners. A finger-tight condition is the torque level of interest for this study.

3 Finite Element Modelling

3.1 Model Assembly

FE models of the single-bolt, single-lap, countersunk composite joints were developed in the nonlinear FE code, Abaqus. Python scripts were written to automate the creation, partitioning and assembling of parts (see Figure 4), allowing the bolt-hole clearance to be varied easily. The laminate secured under the countersunk head is referred to as the *countersunk laminate*, while the other is denoted the *non-countersunk laminate*. The overlapping joint regions were heavily partitioned, including several 'ring regions' (of one ply-thickness) at the hole boundary. This facilitated dense structured meshing in this region of high stress gradients. Including the washer as a separate part allowed the contact conditions of the joint to be modelled more accurately than if it had been integrated in the fastener, as done in a previous study [6].

3.2 Finite Element Mesh, Boundary Conditions & Loading

The finite element mesh is shown in Figure 5, and consists of 3D continuum hexahedral elements. As quadratic elements suffer from inaccuracy in contact modelling [24], linear elements were chosen. However, under bending, the edges of linear elements cannot describe curvature and, through 'shear locking', artificial shear stresses are created [24]. Shear locking can cause joint models to be overly stiff as observed by Ireman [6]. The incompatible modes setting of Abaqus adds degrees of freedom to improve the bending behaviour of fully-integrated linear elements. Linear elements with reduced-integration (C3D8R) could also be used to combat over-stiffness [25], but they suffer from *hourglassing* which can lead to severe mesh distortion in joint models [7]. Consequently, C3D8I elements were used for all regions, conforming to the meshing strategies taken by [13] and [7]. A further possible solution would be to use fully-integrated linear elements with incompatible modes (C3D8I) in regions of high stress gradients, and the less expensive C3D8R elements elsewhere.

The boundary conditions are also shown in Figure 5 and replicate the experiment setup of McCarthy et al. [11]. In the first load step, a 7.2 MPa pre-stress, representing finger-tight torque, was applied to the shank of the bolt using the bolt load tool available in Abaqus/Standard. Displacements were then applied to the joint in the second step. Joint symmetry was not used to reduce the model size, as the presence of off-axis plies leads to an unsymmetrical bolt-hole contact pressure. As in the models of McCarthy et al. [13], light springs were attached to the unconstrained parts (i.e. washer and bolt) to suppress potential rigid body modes. A geometrically linear analysis was employed as the laminates are relatively thick and do not undergo large rotations. Trial analyses accounting for nonlinear geometry, showed the effect on joint response to be very small, though its inclusion adversely affected convergence of this already difficult problem. Laminate rotations in joint models subjected to 5 kN applied load were found to be less than 0.5^0. This is well below 10^0, which is often used as a rule of thumb in deciding whether to account for effects of nonlinear geometry [26]. The effect of joint rotation on the near-hole stress distribution (due to changing contact areas) is essentially included through the use of a finite sliding contact model (see Section 3.4).

3.3 Material Modelling

Two approaches were taken for modelling the HTA/6376 composite material. Firstly, homogenised quasi-isotropic (QI) laminate properties were employed, which do not account for the varying stiffness through the lay-up thickness. These were used to debug contact problems and give a clearer understanding of the behaviour of a single-lap countersunk joint. In subsequent work, each ply was modelled using orthotropic material properties assigned to a single layer of solid elements. The orthotropic properties used for both approaches are shown in Table 2. Ply/lamina properties were obtained from experimental tests and an assumption of transverse isotropy. Homogenised laminate properties were subsequently obtained using FEA and lamination theory. The aim of the current study was to investigate the layer-by-layer elastic stress distributions at boundaries of countersunk holes, so no degradation laws were included. Isotropic, elastic material properties were used for the bolt, nut and washer, see Table 2.

3.4 Contact Description

Contact conditions were enforced by defining contact pairs between interacting surfaces. Slave surfaces were defined, which were unable to penetrate their corresponding master surface. The surface-to-surface discretisation method was employed, which prevents surface penetration in an average sense and generally provides more accurate results than node-to-surface discretisation [24]. McCarthy et al [13] also showed a node-to-surface type setting to result in a flawed radial strain field. Generally master roles were assigned to surfaces of stiffer bodies, which were given coarser meshes. The master and slave assignments are shown in Figure 6. Surfaces were broken down into several contact pairs to avoid the creation of discontinuous surface normals at sharp changes in the geometry. A finite sliding tracking approach was chosen to allow for arbitrary travel of contacting surfaces. The direct contact method, which attempts to strictly enforce a pressure-overclosure relationship [24], was used for enforcing normal contact. A hard pressure-overclosure relationship was chosen for these relatively stiff bodies. Frictionless sliding behaviour was employed, due to the application of only finger-tight torque. A separate trial analysis with typical friction coefficients showed little effect on the results.

Considerable effort was required to obtain a convergent contact solution for these joint models. The main problem encountered was contact chatter, where the status of several slave nodes changed repeatedly between open and

closed. This resulted in severe discontinuity iterations (SDIs) which can prevent convergence. The first approach to mitigate the problem was to include automatic overclosure tolerance [24]. Further improvements in contact convergence were obtained using the unsymmetric solver (recommended due to the highly-curved master surfaces [24]) and contact stabilisation. The amount of contact stabilisation was chosen such that the energy dissipated by viscous damping was negligible. Interestingly, measures normally employed to suppress rigid body modes, such as the use of light springs and contact stabilisation, were also beneficial in mitigating chatter.

4 Results

4.1 Bolt Pre-Load

The finger-tight bolt pre-load, is shown to induce tensile through-thickness stresses (σ_{zz}) in the shank of the fastener, while compressive stresses were observed in the laminate regions under the countersunk head and washer (see Figure 7). Results are shown for the *layered* (not homogenised) models. The magnitudes of the through-thickness stresses were small, ranging from -15 MPa to 23 MPa. The contact pressure between the laminates at the shear plane was found to have decreased to zero at a radial distance of 8mm (one bolt diameter) from the hole edge.

4.2 Joint Deformation (neat-fit case)

The joint deformation at 5 kN applied load is shown in Figure 8. Secondary bending and bolt rotation, both features of single-lap joints, are clearly evident. Figure 9 shows the deformation of the countersunk laminate, with a convex saddling effect observable at the free end. This was previously seen in protruding-head joint models, and attributed to a wide-beam bending effect known as 'tertiary bending' [12]. For the countersunk laminate of Figure 9, (concave) saddling on the non-load-bearing side of the hole (θ=180^0) is negligible compared to that at the free end. This was not the case for the protruding-head models of [12], indicating that the through-thickness contact forces due to impingement of the angled-head are less than those developed under a washer.

4.3 Effect of clearance on load take-up and joint stiffness

Figure 10 (a) shows the load-deflection response for the C1 and C4 clearance cases from the experimental test series [11]. For the C1 (neat-fit) case, there is a slight delay in load take-up (≈10 μm), before the load increases linearly

with further displacement. For the C4 (240 μm) clearance case there is a significant initial delay in load take-up.

Though there is scatter, the earliest load take-up is recorded at approximately 120 μm. This is followed by a

significant non-linear region, before the joint response becomes linear on reaching a load of approximately 1.5 kN. The tendency for load take-up to commence at displacements smaller than the full clearance value contrasted with the protruding-head joints, which exhibited a delay in load take-up equal to the full bolt-hole clearance [12].

The load-deflection response of each of the FE joint models is shown in Figure 10 (b). For increased levels of clearance, the initial delay in load take-up grows, by a similar amount to the experiments. The C4 curve also becomes linear at around 1.8 kN, more or less as in the experiments and the joint stiffness (measured between 2 kN and 7 kN) was found to decrease with hole oversize, also in common with the experiments. The percentage stiffness reductions for the clearance-fit joint models relative to the neat-fit case are shown in Table 3. For the C4 case the joint model predicts a 13.4% reduction in stiffness, while the experimental stiffness drop was 10.8%. The experimentally-measured stiffness drop in the C3 clearance joint is less than that found for the C2 case, which was unexpected and could indicate a degree of experimental error. It should be noted that stiffness calculations are based on full joint deformation measurements on the order of 0.2 mm, which makes the calculations quite sensitive to small errors.

The joint models in general are seen to be significantly stiffer than the experimental results, with the C1 model being 20.7% stiffer than the corresponding value from experiments (24.22 kN/mm). This discrepancy may be in part due to the use of elements with high aspect ratios, caused by the relatively thin plies, as well as the use of linear elements (even with incompatible modes). Other factors are imperfect gripping in the experiments, and uncertainties in measurement of experimental joint stiffness, as discussed by Lawlor [21]. For instance, slight warping was found in the washers due to the punching nature of the manufacturing process. This was found to result in greater compliance in the joint response, as the slightly curved washers were 'flattened' during loading. In any case, the models capture the main phenomena of the tests, and give good comparative indications of the effects of variable-clearance.

The load-deflection curves in the clearance-fit joints exhibit three distinct phases in the initial load take-up region. This is explained by examining the bolt position at each phase, as shown for the C4 joint model in Figure 11. In the first phase, the countersunk laminate and bolt slide as a unit (to the right), reducing the clearance between the bolt and the non-countersunk laminate. Once contact occurs between the bolt and the non-countersunk laminate, initial load take-up occurs and the second phase begins. During this the countersunk laminate slides relative to the bolt, as its cylindrical part (t_{cyl} in Figure 3) makes contact with the bolt. At this point clearances with respect to both

laminates are closed and the joint becomes significantly stiffer (phase 3). This behaviour differs from protruding-head joints, where both clearances close before any load transfer [12].

Beyond 2 kN load, the FE C4 model, which has linear elastic properties, shows slight stiffening (attributed to the growth in contact area with load). This stiffening is not seen in the corresponding experimental curves (Figure 10 (a)). As stated in McCarthy and McCarthy [12] for protruding-head models, this is most likely due to damage development in the experimental tests resulting in stiffness reduction which cancels out the stiffness increase due to the growing contact area.

4.4 Effect of clearance on stress distribution around the hole boundary

4.4.1 Results from using *homogeneous* material properties

To investigate the stress distribution at the hole boundary, the stresses were extracted from the integration points closest to the hole edge (≈25 μm distance), at an applied load level of 5 kN. Of primary interest were the radial and tangential stresses. High radial stresses would be expected to promote bearing damage, while high tangential stresses promote net-tension failure. Stresses in the *homogeneous* models are detailed in this section.

Figure 12 shows the radial and tangential stress distributions found in the non-countersunk laminate of the C1 joint, and are similar to those observed in the laminates of the C1 protruding-head joint models by McCarthy and McCarthy [12]. The highest radial stress is at the shear plane, peaking at the joint centreline. It is noted that this is a region of singularity in the numerical model, as the rotated bolt experiences a line contact with the hole edge [13]. The highest tangential stresses are also found at the shear plane, with the peaks occurring at angular positions of $\theta = \pm 80°$, corresponding to the end of the contact region (where radial stress has dropped to zero). The magnitude of the radial stress peak (≈ 480 MPa) is higher than the tangential stress peaks (≈ 290 MPa), which has also been observed for pin-loaded and protruding-head models by Kelly and Hallström [10] and protruding-head models by McCarthy and McCarthy [12].

The radial and tangential stresses in the countersunk laminate of the C1 and C4 joints are provided in Figure 13, and are found to be significantly different to those developed in the non-countersunk laminate. In Figure 13 (a), which shows the radial stress in the C1 countersunk laminate, it can be seen that significant radial stress exists only over the cylindrical thickness (t_{cyl}) region (0 to ~1.6 mm from the shear plane), with low radial stress values found in the countersink region of the hole. Thus the bearing load is transferred almost entirely through the cylindrical part, which is in agreement with Ireman [6]. The only exception is near the outer surface of the laminate (5.2 mm from the shear plane), where small radial stress peaks appear from +/-90^0 to 180^0. This is due to the countersunk head impinging on the angled-hole at $\theta=180^0$ (non-load bearing side). Over the t_{cyl} region, there is the expected peak in radial stress at the shear plane, similar to the non-countersunk laminate, but there is also a second peak at the intersection of the countersink with the cylindrical part of the hole; in fact this is the location of the largest radial stress. This is caused by an edge contact situation between the countersunk bolt and this intersection. The tangential stresses in the t_{cyl}

region (i.e. near the shear plane) are higher than the values in the non-countersunk laminate, though not as much so as in the radial stress case. Differently from radial stresses, significant tangential stresses do exist in the countersunk region of the laminate, although a sharp reduction in the magnitude begins at the angle-shank intersection.

Given the higher radial and tangential stresses at the countersunk hole, the countersunk laminate is the critical one from a strength analysis viewpoint. This makes it the main focus of the variable-clearance study. Figure 13 (c) shows the radial stress state in the countersunk laminate for the C4 (240 μm) clearance case. The radial stress is seen to be much more localised than in the C1 case, with a $\theta = \pm 35^0$ contact arc at the shear plane. The high radial stresses (and thus strains) are an indication that the bolt, making contact over a reduced contact arc, creates a deeper indentation near the shear plane, implying greater bolt rotation. Increased bolt rotation leads to greater interaction between the angled surfaces, giving significant radial stresses in the angle-region of the hole which were not seen for the C1 clearance case. This means that unlike the neat-fit clearance case, the countersunk region of the hole reacts a substantial part of the bearing load, resulting in a reduced radial stress peak at the angle-shank intersection. In fact the maximum radial stress in the C4 joint is *less than* in the C1 joint, which is completely at odds with findings of previous researchers who have only dealt with protruding head or pin-loaded joints.

In Figure 13 (d), the C4 tangential stress peaks have moved closer together due to the reduced contact arc, but the effect of the increased clearance on the tangential stress distribution is not as pronounced as in the radial stress case. Previous authors have shown this in modelling of pin-loaded laminates [8, 10] and protruding-head joints [12].

4.4.2 Results from using *layered* material properties

In this section stresses in each ply are extracted from the *layered* models at a load level of 5 kN. The layers are numbered 1-40 beginning at the shear plane.

Figure 14 shows the radial stress for the C1 (neat-fit) joint. All values are negative, as the bolt-hole contact pressure causes in-plane compression of the plies. Significant radial stresses occur between $\theta = \pm 80^0$, showing a similar contact area to the homogenous model. In each layer, the peak radial stress occurs near to where the ply is (radially) stiffest, e.g. near +45º for the +45º plies (not exactly at +45º as the pressure falls away from its peak in the 0º position). The radial stress is essentially zero under the angled-head. Thus, virtually all the bearing load is carried by the limited number of plies which are in contact with the cylindrical shank of the bolt (i.e. those in the t_{cyl} region). The 0^0 plies, which are in line with the loading direction, exhibit the highest stress peaks, and are the most effective in carrying the axial joint load. For comparison, the radial stress distribution in the protruding-head model of McCarthy et al. [12] is provided in the inset to Figure 14. The peak radial stresses in the countersunk joint are about 1.7 times those in the protruding-head joint. In [11], these same joints were tested experimentally, and the 2% offset strength was 529.8 MPa for C1 protruding head joints and 347.7 MPa for C1 countersunk joints, the ratio of which is 1.52. Thus, the higher radial stress correlates well with its lower strength, indicating that radial stress in the 0^0 ply

closest to the shear plane is the dominant stress component determining failure in the neat-fit clearance case. The situation is not as clear-cut in the higher clearance case, as will be shown later.

The other noticeable point from Figure 14 is that in the protruding-head joint there is a gradual drop-off in radial stress in moving away from the shear plane, whereas in the countersunk joint, the peaks in the two 0^0 (or 45^0 & -45^0) plies have nearly the same value. This correlates well with the double-peak in radial stress over the t_{cyl} region seen in the homogeneous models in Figure 16(a). The fact that the bearing load is fairly evenly distributed among the plies of the t_{cyl} region suggests that when a significant failure event occurs in the countersunk laminate, it may cause a more sudden load drop than that seen in laminates of protruding-head joints, due to the likelihood of multiple ply failures occurring simultaneously. This, in fact, is borne out by the experimental results from [11], shown in Figure 15. It can be seen that for two of the three tested countersunk joints show a distinct 'knee' in the load-deflection curves at initial failure, whereas no such kink was evident in the protruding-head joint results.

Figure 16 shows the tangential stresses for the C1 joint at 5 kN applied load. In each ply, the peak value occurs at an angular position where the fibre direction of the ply is tangential to the hole edge (as observed by McCarthy and McCarthy [12] and Kelly and Hallström [10]). There is again a significant drop-off in the tangential stresses at the end of the t_{cyl} region. Negative tangential stresses at certain locations are attributed to the hole becoming locally oval-shaped, as observed by McCarthy and McCarthy [12] and Naik and Crews [9].

The radial stress distribution for the C4 clearance case is shown in Figure 17. As seen for the homogeneous model, significant radial stress is only observed over a contact arc of $+/-35^0$ at the shear plane. This limited contact area leads to the 0^0 ply closest to the shear plane experiencing a very high radial stress (1875 MPa compared to 1430 MPa in the C1 case). This would seem to indicate that the C4 joint should fail in bearing at a significantly lower load than the C1 joint, in agreement with the perceived wisdom on the effects of clearance from multiple previous studies. However, this was not the case for the experimental results in [11], and to explain why, one needs to consider more than just the radial stress. The second observation concerning Figure 17 is the drop-off in radial stress in moving away from the shear plane, which is not evident in the C1 joint (Figure 14). This is also in line with the homogeneous models, where it was seen that the "second peak" at the angle-shank intersection was suppressed in the C4 model (Figure 13(c)) compared to the C1 model (Figure 13 (a)). This latter effect would be expected to produce a less dramatic load drop at first failure in the C4 joint, since an initial failure in the 0^0 ply nearest the shear plane, would promote load take-up in other plies, through increased bolt rotation which results in a greater area of bolt-hole contact. This was in fact borne out in the experimental data of [11] which showed less evidence of kinks in the load-deflection curves of C4 countersunk joints than in those with C1 clearance.

Tangential stress at the C4 clearance countersunk hole is shown in Figure 18. The stress distribution looks similar to the neat-fit case shown in Figure 16, except the peak stresses in the $+/-45^0$ plies are now seen to be higher than those in the 0^0 plies. This supports observations of previous studies, which found the location of peak tangential stress moved towards the bearing plane ($\theta=0^0$) with increasing clearance [9, 12, 27, 28], and was also observed for the homogeneous models. Since the joints were designed to fail in bearing, the magnitudes of tangential stresses are not of particular interest.

While in-plane stresses give some indication of failure load, experimental studies have shown joint bearing strength depends on the level lateral constraint. Thus, through-thickness stress is an important factor. In [11], 2% offset bearing strength was measured experimentally for each of the four clearance-joints in Table 1. Surprisingly, each of the C2, C3 and C4 clearance cases exhibited higher 2% offset bearing strength than the C1 case. For the protruding-head joints in [11], a drop in strength with increasing clearance was observed, which is much more in line with expectations and previous results. In the C4 countersunk laminate, the 0^0 ply closest to the shear plane experiences a very high radial stress (1875 MPa compared to 1430 MPa in the C1 case). This would seem to indicate that increasing clearance should lead to decreased 2% offset strength. To explain the increase in strength with clearance, the through-thickness stress distributions are considered.

Through comparisons with the work of McCarthy and McCarthy [12], the stress distributions in the non-countersunk laminates here were found to be very similar to (and thus considered representative of) those in the laminates of a protruding-head joint. The through-thickness stresses in the non-countersunk laminate are plotted in Figure 19. Significant compressive through-thickness stresses are observed, which peak at 180^0 (the non-loaded side of the hole). The magnitude of the compressive stress from -90^0 to 90^0 (the loaded side of the hole) is small. With larger clearance (Figure 19 (b)) the magnitude of the stress grows significantly but this will not affect the bearing failure of the joint, since the damage develops on the other side of the hole. Figure 20 shows the stresses in the countersunk laminate. In this case, significant compressive through-thickness stresses *are* evident between $+90^0$ and -90^0 (the loaded side of the hole) largely in the t_{cyl} region. These compressive stresses will help *delay* the onset of bearing failure by providing lateral restraint to the plies and suppressing "brooming". Furthermore, the magnitude of these helpful stresses is *tripled* in the C4 joint (Figure 20 (b)). This indicates that even though clearance significantly increases the radial stress acting at the hole boundary, this can be counteracted by the increased level of lateral constraint offered in this region. This helps to explain the increase in 2% offset strength with clearance seen in the experiments of [11].

This difference between protruding head and countersunk joints is related to the displacement of the protruding-head and countersunk fastener. As illustrated in Figure 21, it can be seen that the protruding-head joint provides little lateral constraint at the load-bearing side of the joint (in fact the bolt head has lifted away from the washer). This contrasts with the countersunk fastener which is shown to constrain the laminate at the damageable region of the hole. In a microscopy study of both joints following bearing failure, delamination was only present in the failed laminates of the protruding-head joints [21] (see Figure 21 (a)). We see that for the protruding-head joint, there is significant 'brooming' of the laminate, in addition to the damage at the shear plane. This correlates with the lack of lateral constraint at the damaging boundary of the hole. The countersunk laminate exhibits only compression and shearing damage along with fibre/matrix chip-outs, with brooming appearing to be suppressed.

5 Conclusions

In this paper, the mechanical behaviour of single-lap composite joints secured with finger-tight countersunk fasteners were investigated in detail. Stress distributions at the boundary of the countersunk hole were presented for varying degrees of clearance. The results showed that where the countersunk hole is oversized, the contact area is reduced, resulting in higher radial stresses, and a reduction in joint stiffness. Reductions in the joint model stiffness correlated

reasonably well with the experimental data. Generally the angled part of the hole was found to be ineffective in transmitting load, and a limited number of plies carried the majority of the load in the countersunk laminate. This localised form of load transfer explained the lower bearing strengths of countersunk joints compared to those with protruding-head fasteners and the significant 'knee' found in experimental load-deflection curves.

The increase in radial stress shown for high clearance countersunk joints had previously been observed for protruding-head joints. However, while protruding-head joints in experiments demonstrated an associated reduction in bearing strength, countersunk joints did not. The final section of the work addressed this apparent inconsistency, by investigating the through-thickness stresses at the hole boundary. Significant compressive through-thickness stresses were found in the most damageable region of these finger-tight countersunk joints, and the stress magnitudes increased with clearance. These compressive stresses, indicating lateral constraint, have the potential to offset the weakening effect of the reduced contact area due to clearance, explaining the *elevated* bearing strengths of clearance-fit countersunk joints.

In comparison to previously published numerical work on countersunk joints [6, 7, 29], the results shown here provide a highly-detailed representation of the stress state at the countersunk hole boundary, which governs joint failure. The need for a 3D FE analysis was affirmed through the presence of non-uniform, in-plane stress distributions and significant through-thickness stresses at the hole boundary. Numerical modelling of variable-clearance in countersunk composite joints could not previously be found in open literature. Future work will employ a continuum damage model and investigate the behaviour of countersunk joints subjected to high-speed loading.

Acknowledgement

The authors wish to acknowledge the Irish Research Council for Science Engineering and Technology (IRCSET) and the SFI/HEA Irish Centre for High-End Computing (ICHEC) for the provision of financial support and computational facilities.

References

[1] McCarthy MA. BOJCAS: Bolted Joints in Composite Aircraft Structures. Air Space Eur. 2001;3:139-42.
[2] Pearce G, Johnson A, Thomson R, Kelly D. Experimental Investigation of Dynamically Loaded Bolted Joints in Carbon Fibre Composite Structures. Appl Compos Mater. 2010;17:271-91.
[3] Hart-Smith LJ. Bolted Joints in Graphite-Epoxy Composites. 1976.
[4] Shyprykevich P. Characterization of bolted joint behaviour: MIL-HDBK-17 Accomplishments at Standardization. JCTRER. 1995;17:260-70.
[5] Ekh J. Multi-Fastener Single-Lap Joints in Composite Structures. Stockholm: Royal Institute of Technlology, 2006.
[6] Ireman T. Three-dimensional stress analysis of bolted single-lap composite joints. Compos Struct. 1998;43:195-216.
[7] Hühne C, Zerbst AK, Kuhlmann G, Steenbock C, Rolfes R. Progressive damage analysis of composite bolted joints with liquid shim layers using constant and continuous degradation models. Compos Struct. 2010;92:189-200.
[8] DiNicola AJ, Fantle SC. Bearing Strength Behaviour of Clearance-Fit Fastener Holes in Toughened Graphite/Epoxy Laminates. Composite Materials: Testing and Design ASTM STP 1206. 1993;11:220-37.
[9] Naik RA, Crews JH. Stress Analysis Method for a Clearance-Fit Bolt Under Bearing Loads. AIAA J. 1986;24:1348-53.
[10] Kelly G, Hallström S. Bearing strength of carbon fibre/epoxy laminates: effects of bolt-hole clearance. Compos Part B-Eng. 2004;35:331-43.

[11] McCarthy MA, Lawlor VP, Stanley WF, McCarthy CT. Bolt-hole clearance effects and strength criteria in single-bolt, single-lap, composite bolted joints. Compos Sci Technol. 2002;62:1415-31.
[12] McCarthy CT, McCarthy MA. Three-dimensional finite element analysis of single-bolt, single-lap composite bolted joints: Part II--effects of bolt-hole clearance. Compos Struct. 2005;71:159-75.
[13] McCarthy MA, McCarthy CT, Lawlor VP, Stanley WF. Three-dimensional finite element analysis of single-bolt, single-lap composite bolted joints: part I--model development and validation. Compos Struct. 2005;71:140-58.
[14] Stockdale JH, Matthews FL. The effect of clamping pressure on bolt bearing loads in glass fibre-reinforced plastics. Composites. 1976;7:34-8.
[15] Collings TA. The strength of bolted joints in multi-directional cfrp laminates. Composites. 1977;8:43-55.
[16] Eriksson I. On the Bearing Strength of Bolted Graphite/Epoxy Laminates. J Compos Mater. 1990;24:1246-69.
[17] Sun H-T, Chang F-K, Qing X. The Response of Composite Joints with Bolt-Clamping Loads, Part II: Model Verification. J Compos Mater. 2002;36:69-92.
[18] Park H-J. Effects of stacking sequence and clamping force on the bearing strengths of mechanically fastened joints in composite laminates. Compos Struct. 2001;53:213-21.
[19] Nassar SA, Virupaksha VL, Ganeshmurthy S. Effect of Bolt Tightness on the Behavior of Composite Joints. J Press Vess. 2007;129:43-51.
[20] Niu MC. Airframe Stress Analysis and Sizing. 2nd ed. Hong Kong: North Point, 1999.
[21] Lawlor VP. An Experimental Study of the Effects of Variable Bolt-Hole Clearance on the Mechanical Behaviour of Composite Bolted Joints [PhD]: University of Limerick, 2004.
[22] Camanho PP, Matthews FL. Stress analysis and strength prediction of mechanically fastened joints in FRP: a review. Composites Part A: Applied Science and Manufacturing. 1997;28:529-47.
[23] McCarthy MA, Lawlor VP, O'Donnell PC, Harris K, Kelly P, Cunningham JP. Measurement of Bolt Pre-load in Torqued Composite Joints. Strain. 2005;41:109-12.
[24] Abaqus-Inc. Abaqus User Manual, Version 6.9 Dassault Systèmes Simulia Corp, Providence, RI, USA. 2009.
[25] Camanho PP, Matthews FL. Delamination Onset Prediction in Mechanically Fastened Joints in Composite Laminates. J Compos Mater. 1999;33:906-27.
[26] Bower AF. Applied Mechanics of Solids: CRC Press, 2010.
[27] Hyer MW, Klang EC, Cooper DE. The Effects of Pin Elasticity, Clearance, and Friction on the Stresses in a Pin-Loaded Orthotropic Plate. J Compos Mater. 1987;21:190-206.
[28] Ko HY, Kwak BM. Contact analysis of mechanically fastened joints in composite laminates by linear complementarity problem formulation. Compos Struct. 1997;40:187-200.
[29] Chishti M, et al. Progressive damage in single lap countersunk composite joints. IOP Conference Series: Materials Science and Engineering. 2010;10:012064.

Figure Captions:

Figure 1 Countersunk joint geometry.

Figure 2 (a) Countersink head geometry and related cylindrical thickness (t_{cyl}) (b) Effect of clearance on t_{cyl}.

Figure 3 (a) Fibre orientation (α) and angular position (θ) on hole boundary (b) Polar coordinate system for analysing the hole boundary stresses.

Figure 4 Parts created to assemble the joint model, showing partitioning strategy.

Figure 5 Finite element model (partially cut), showing mesh and boundary conditions.

Figure 6 Master and slave surfaces used to define contact pairs.

Figure 7 Through-thickness stresses developed in the bolt region after application of the finger-tight bolt pre-load (C1 clearance).

TABLES:

Table

Clearance code	**Nominal clearance**	**Reamer diameter**		**Bolt diameter**		**Possible clearance**		**t_{cyl} (micrograph images)**
	(μm)	Min (mm)	Max (mm)	Min (mm)	Max (mm)	Min (μm)	Max (μm)	(mm)
C1	0 (Modelling: 10)	7.985	7.994	7.972	7.987	-2	22	1.43 (11 plies)
C2	80	8.065	8.074	7.972	7.987	78	102	1.43 (11 plies)
C3	160	8.145	8.154	7.972	7.987	158	182	1.56 (12 plies)
C4	240	8.225	8.234	7.972	7.987	238	262	1.69 (13 plies)

Table2

	E_{11} (GPa)	E_{22} (GPa)	E_{33} (GPa)	G_{12} (GPa)	G_{13} (GPa)	G_{23} (GPa)	ν_{12}	ν_{13}	ν_{32}
Lamina	140	10	10	5.2	5.2	3.9	0.3	0.3	0.5
Homogenised Laminate (QI)	54.25	54.25	12.59	20.72	4.55	4.55	0.309	0.332	0.332
	E (GPa)	ν							
Titanium (Bolt)	110	0.29							
Steel (Washer & Nut)	210	0.3							

Table3

Clearance	C1	C2	C3	C4
Model stiffness (kN/mm)	29.24	28.17	26.68	25.32
Percentage change from C1 (models)	-	-3.7%	-8.8%	-13.4%
Percentage change from C1 (experiments)	-	-5.2%	-4.0%	-10.8%

Figure1

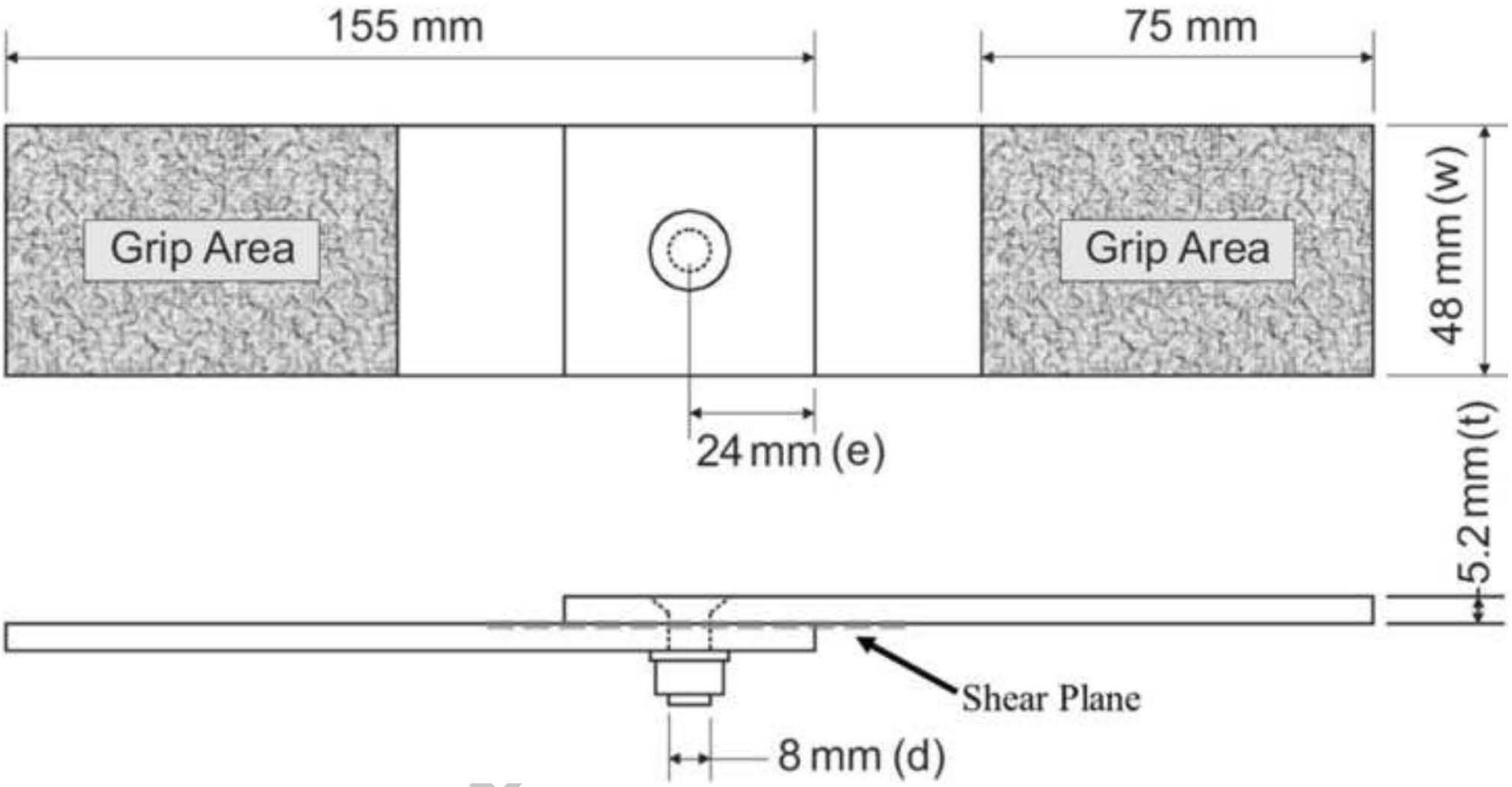

Figure2

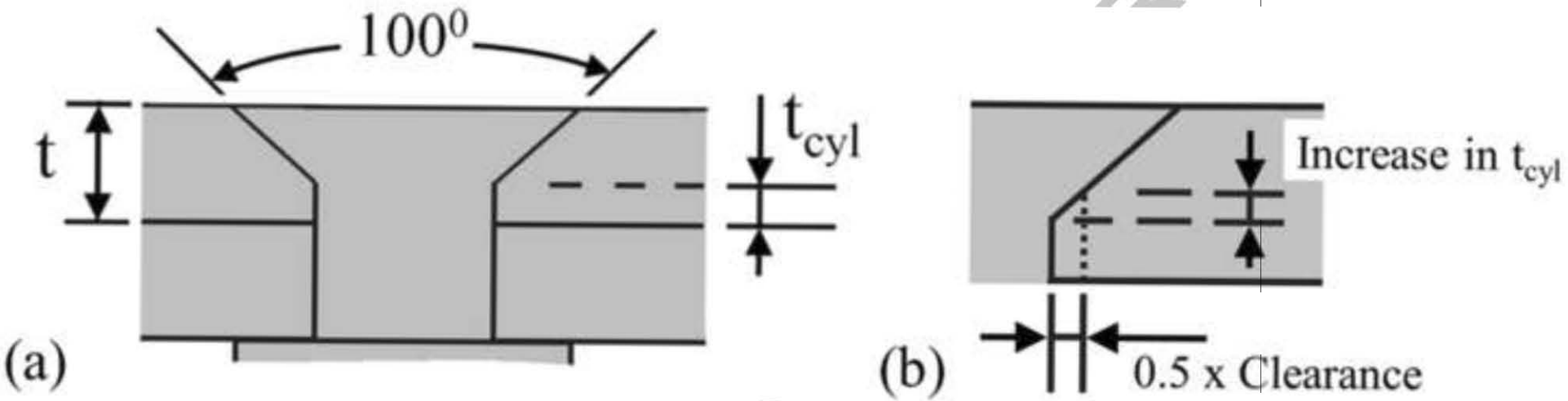

Figure3

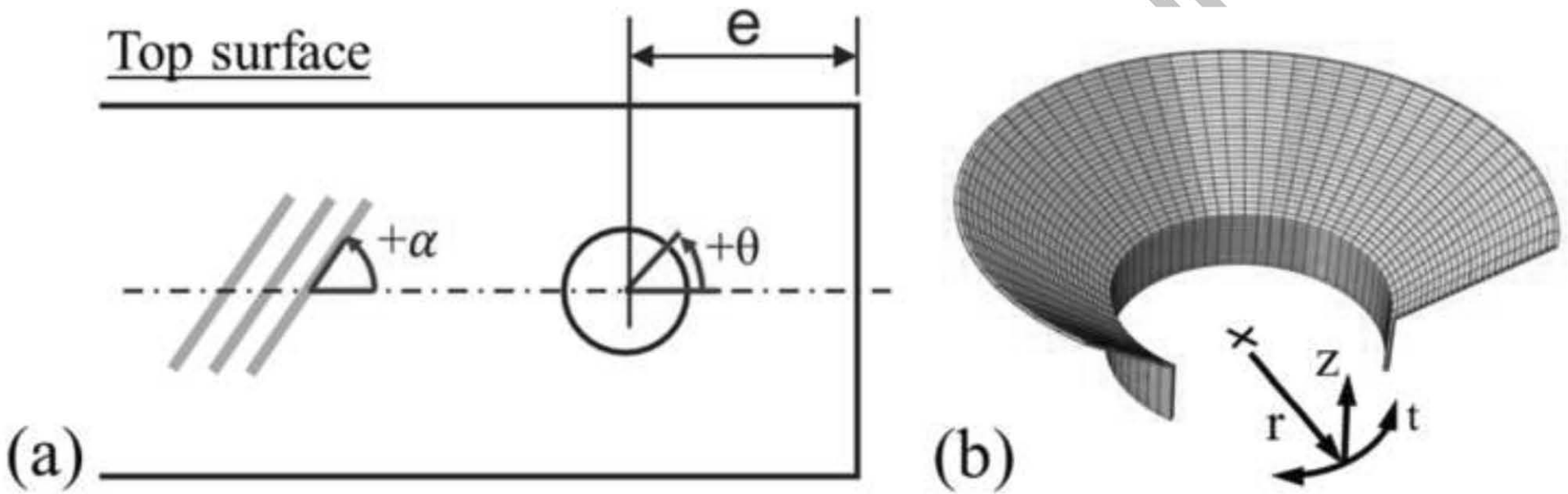

Figure4

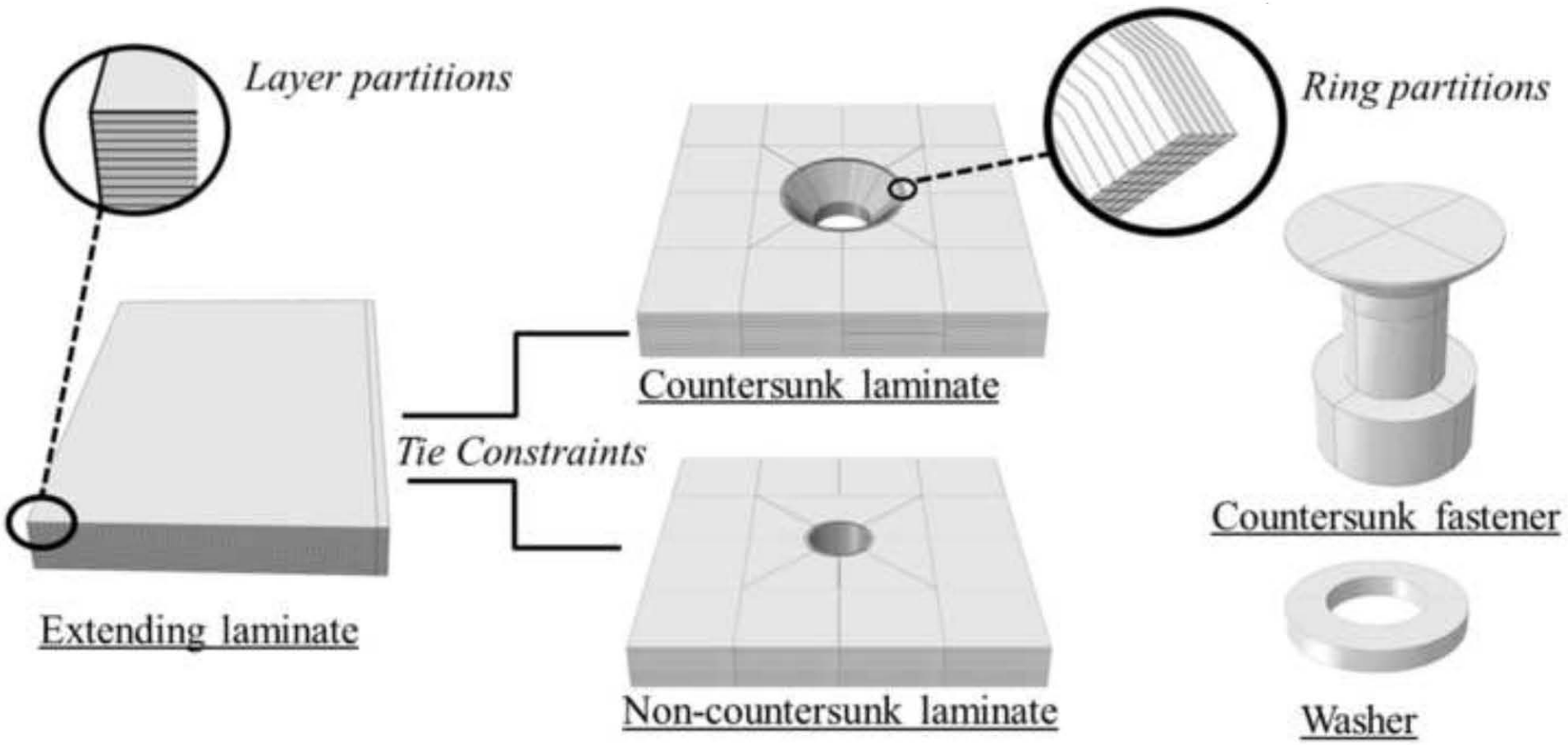

Figure5

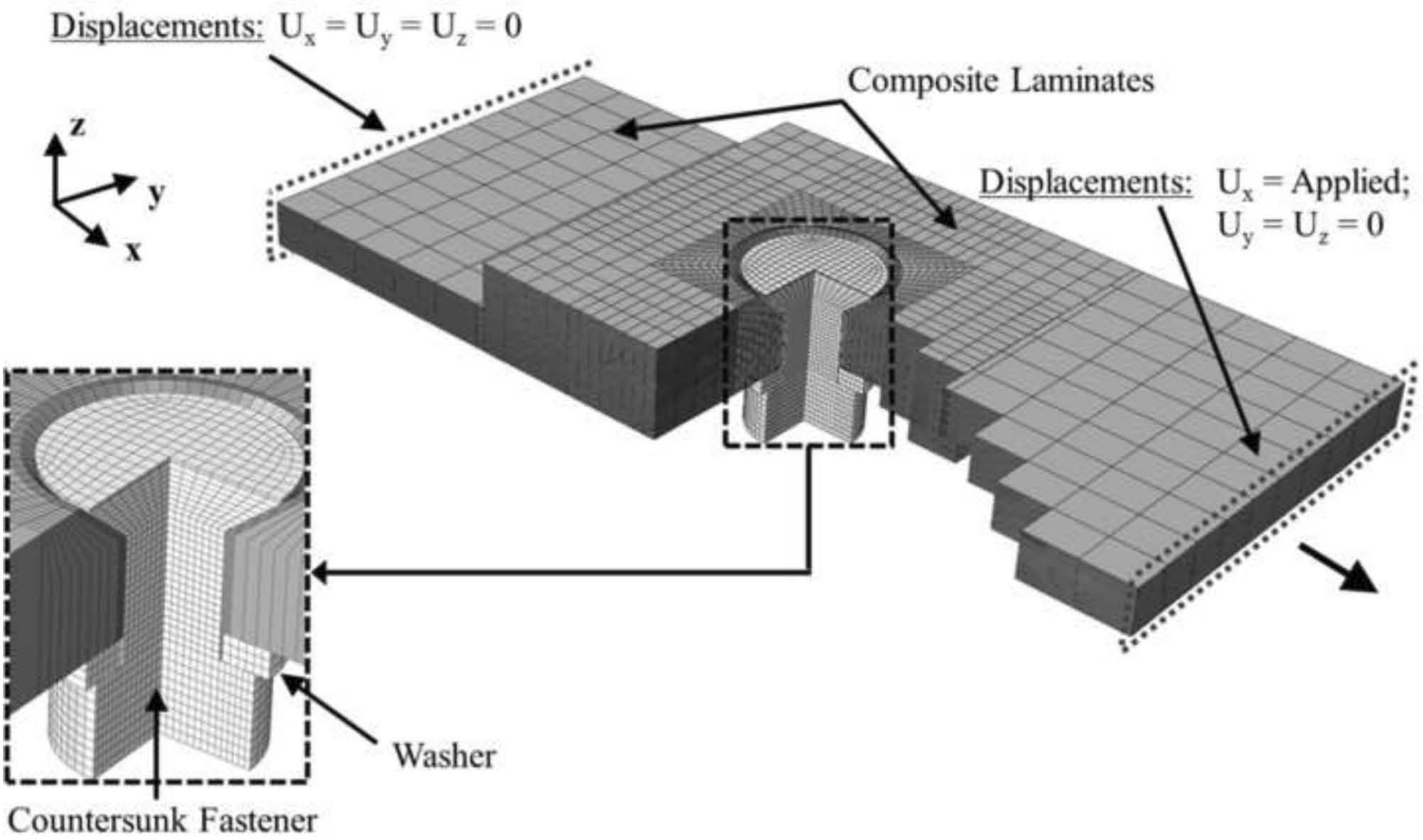

Figure6

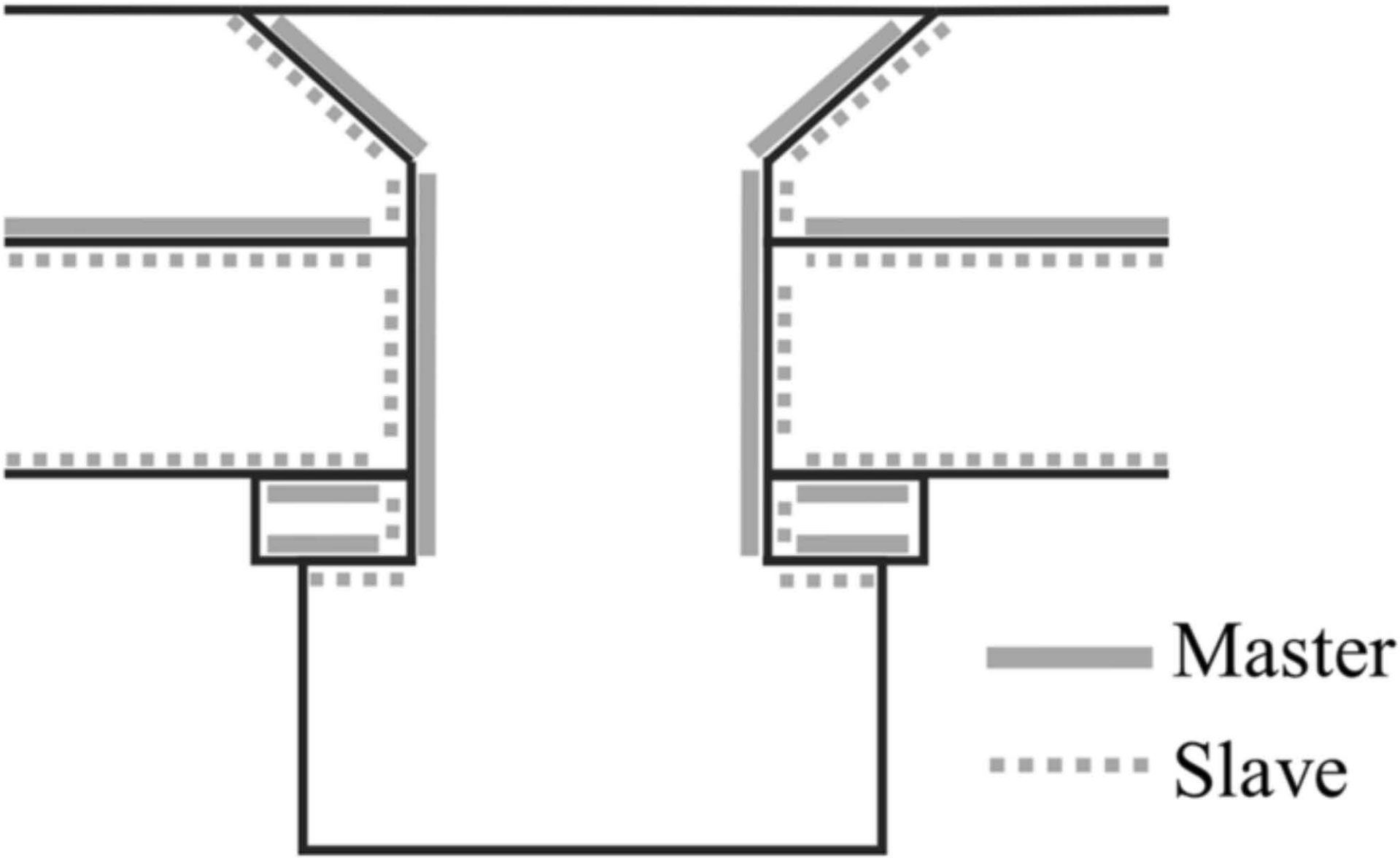

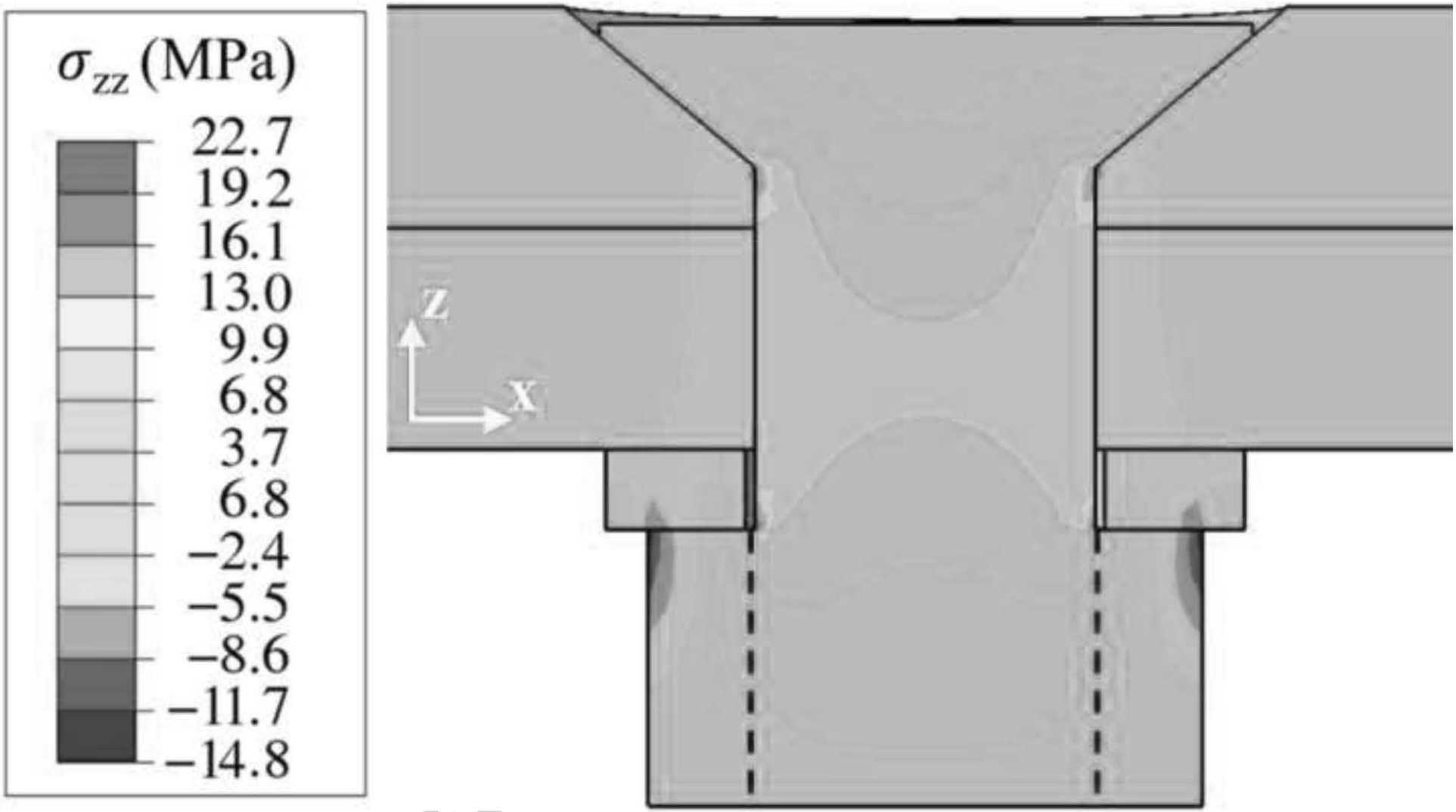

Figure8

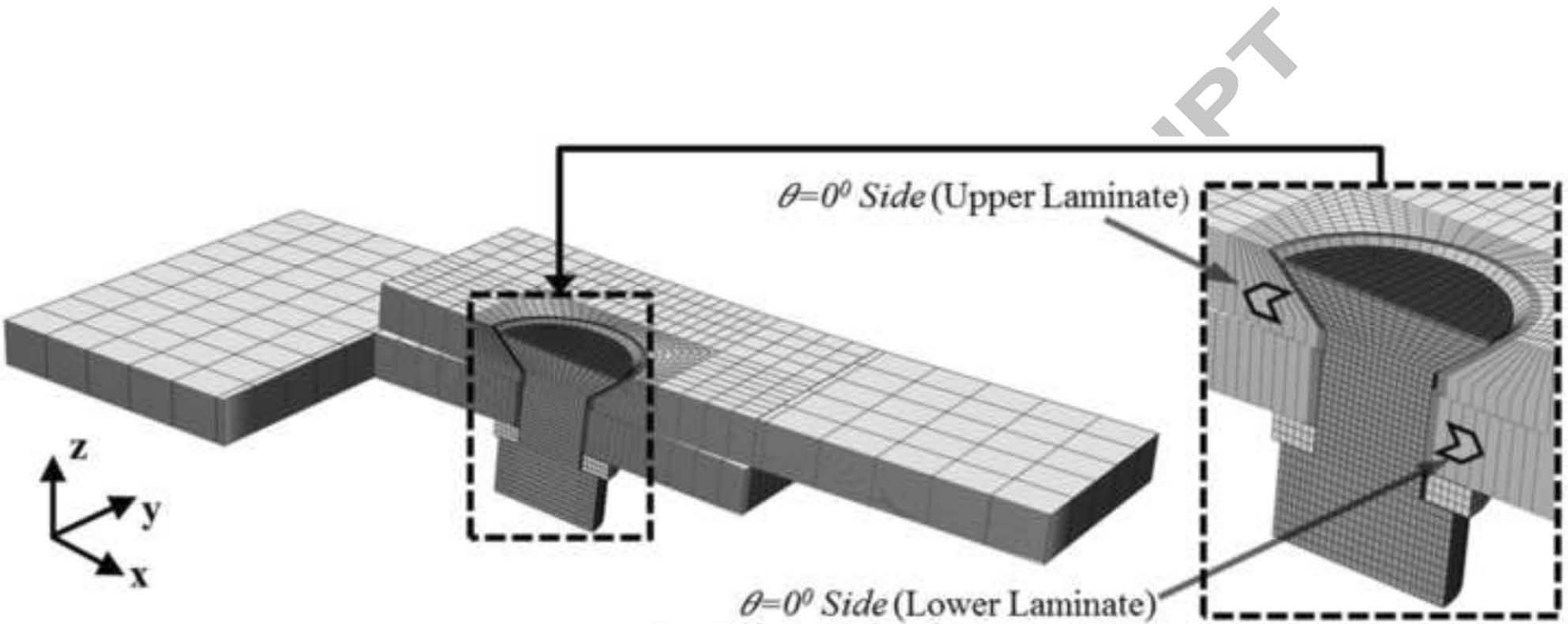

Figure9

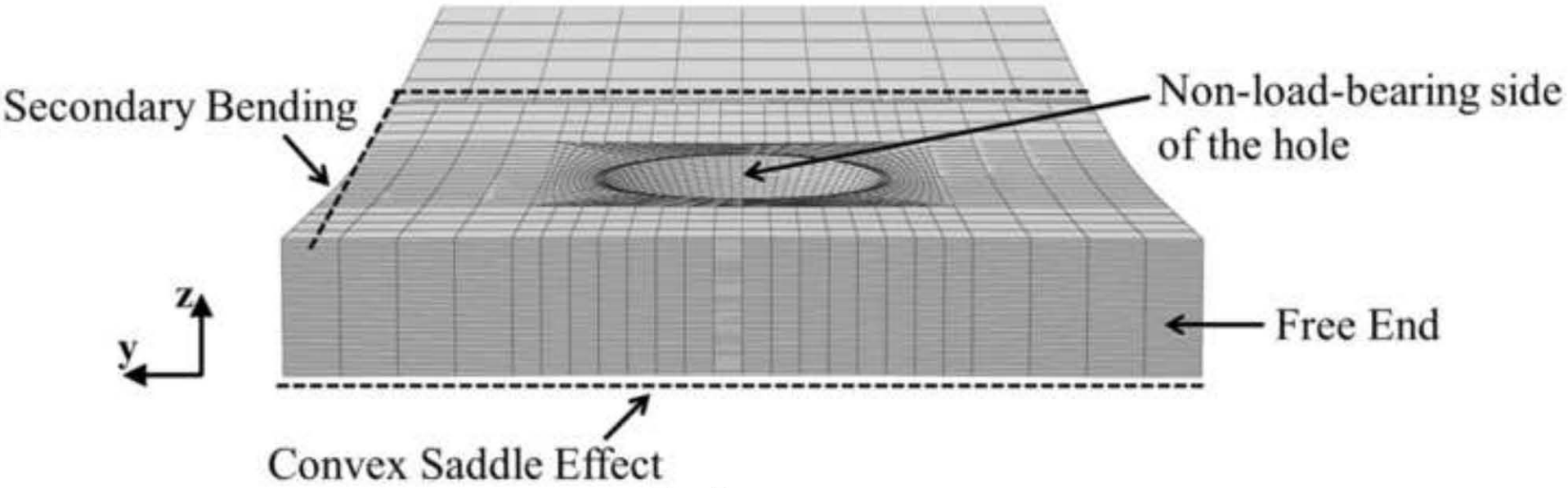

Figure10

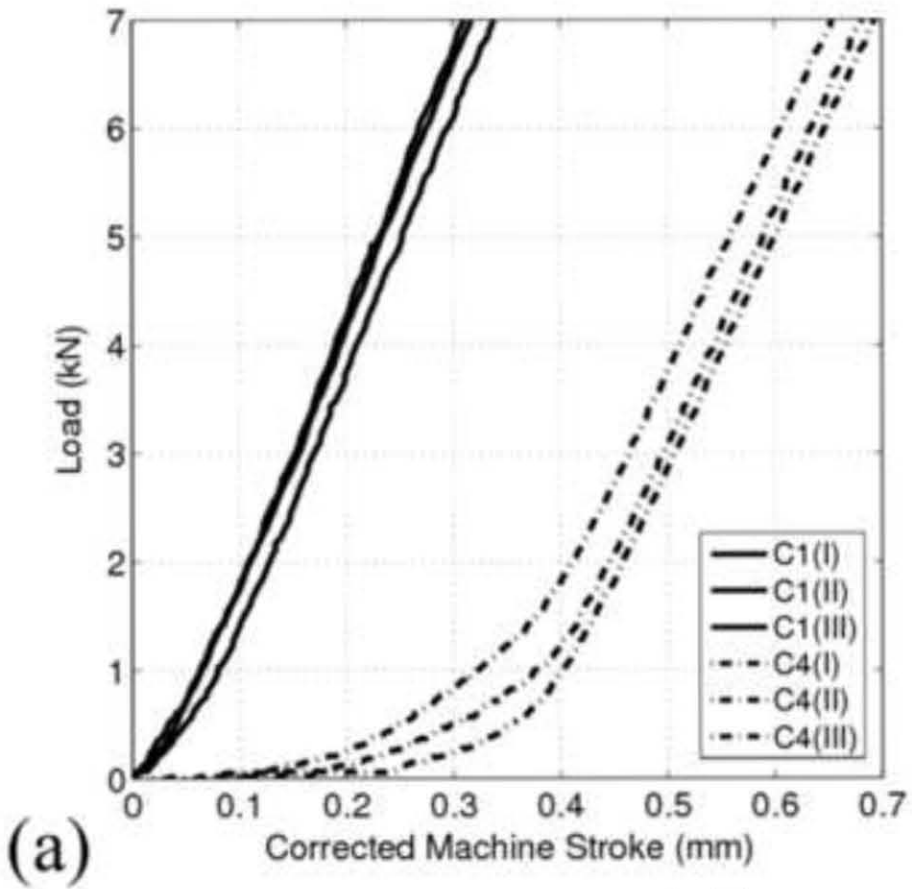

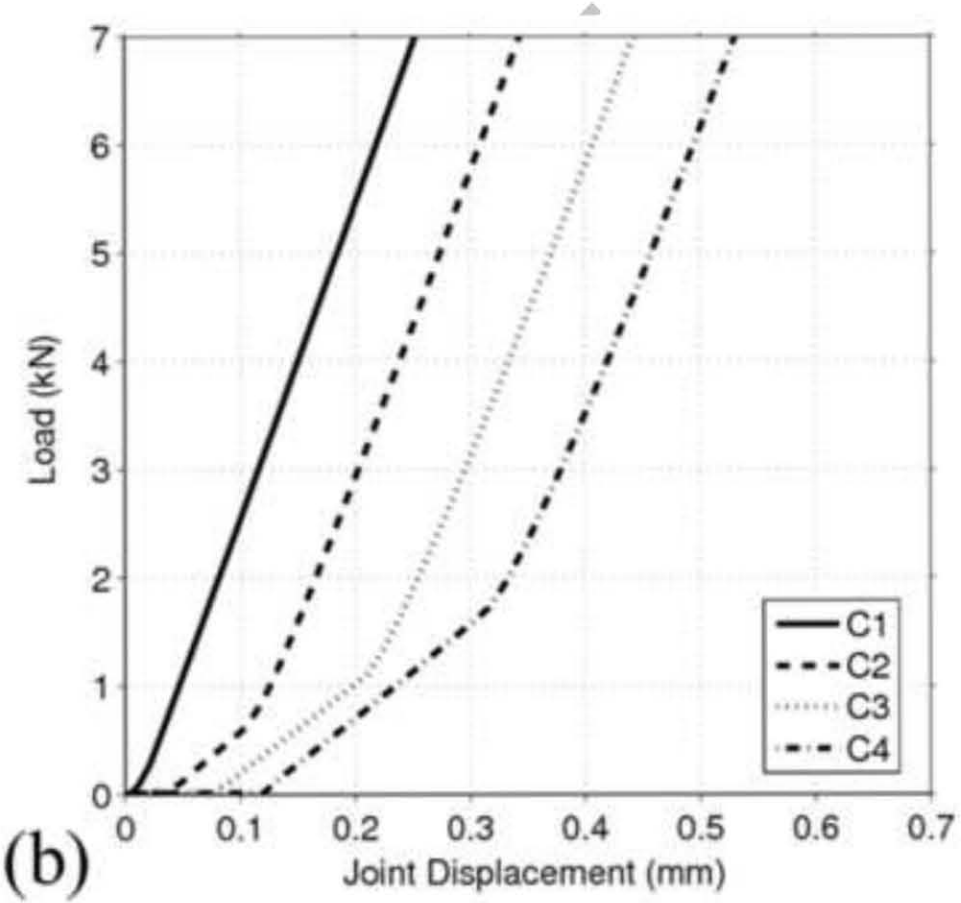

Figure11

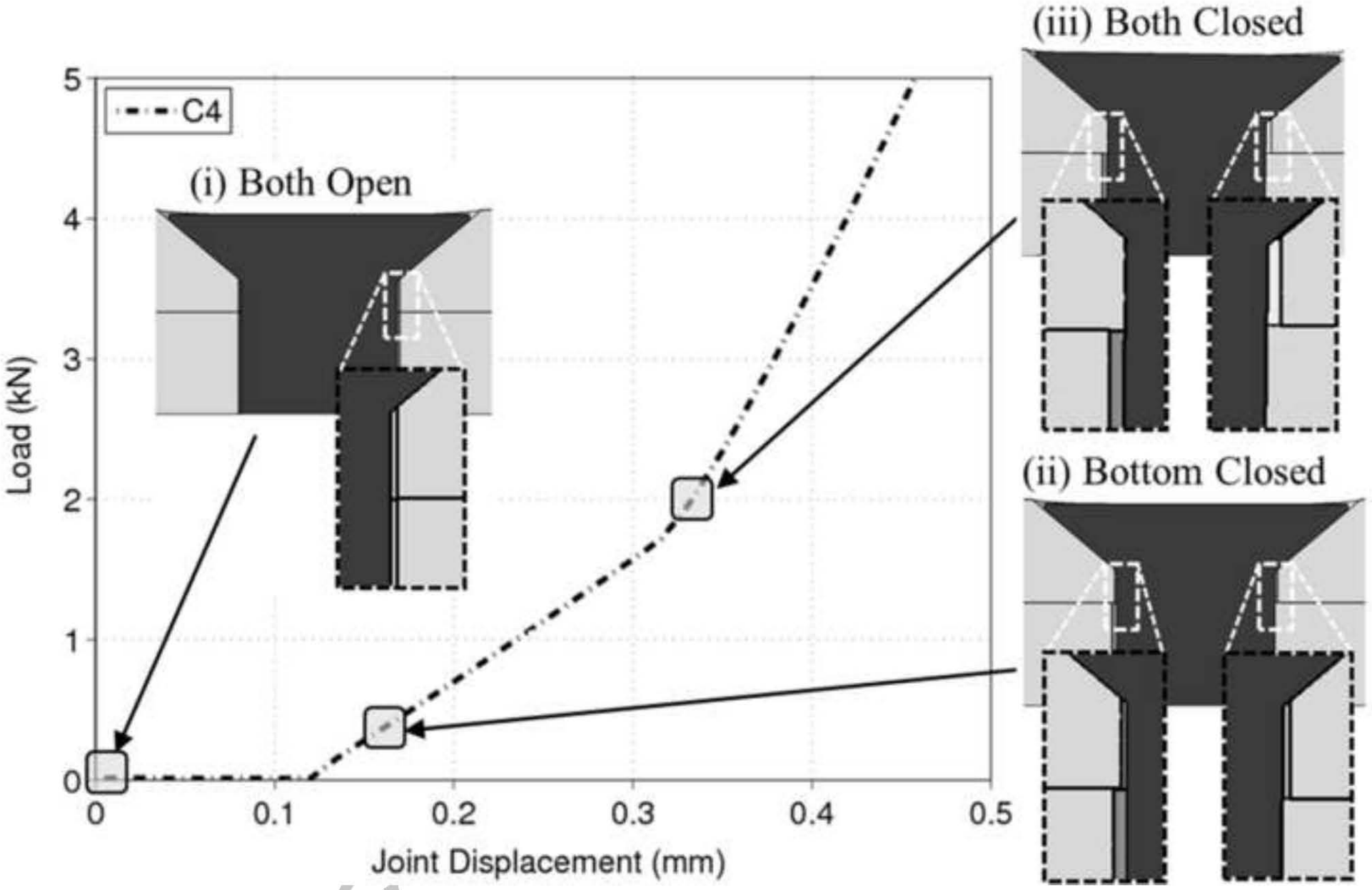

Figure12

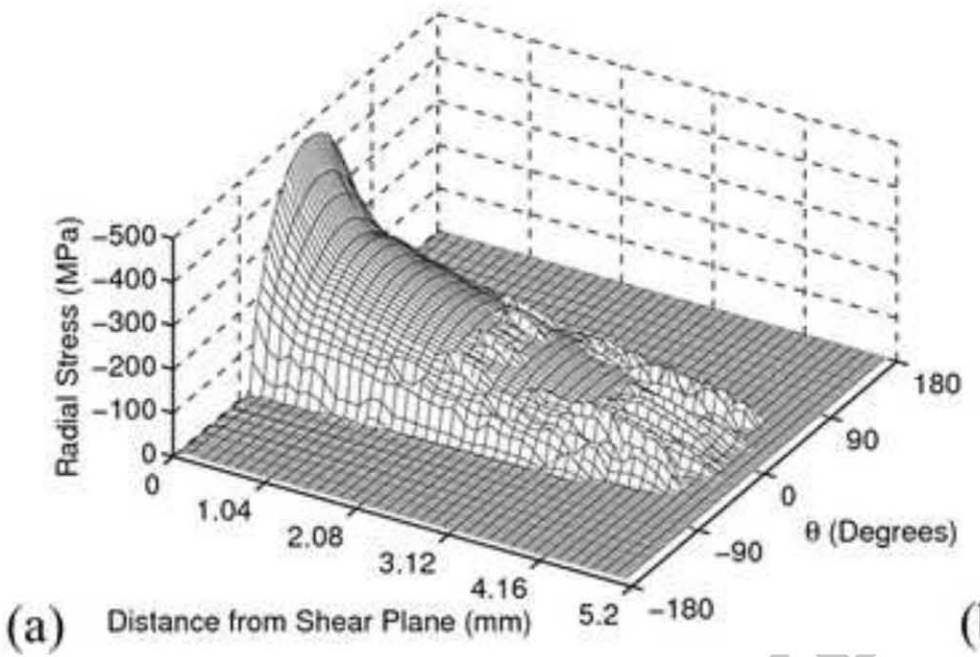

(a)

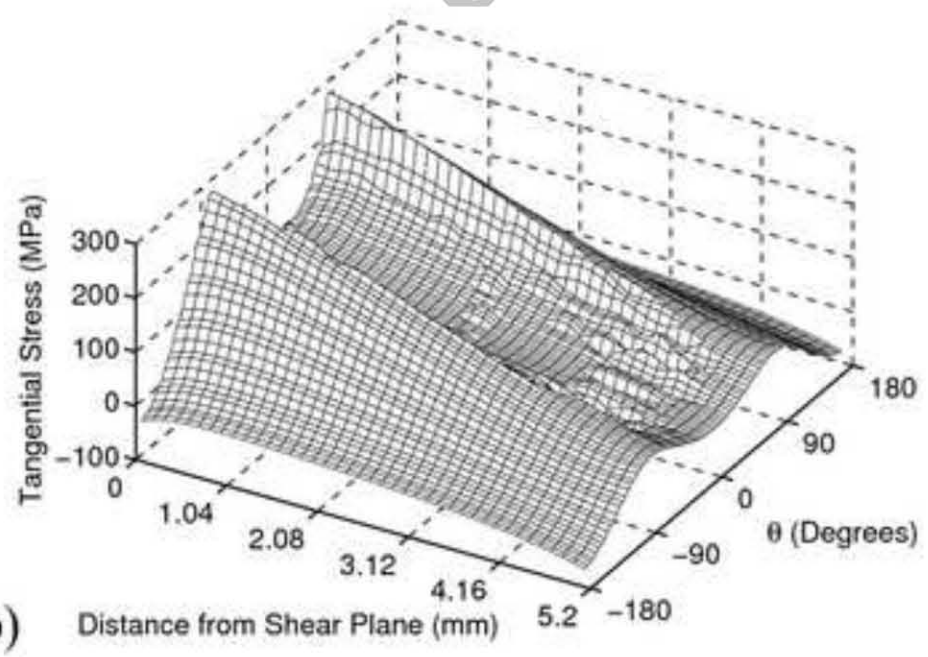

(b)

Figure13

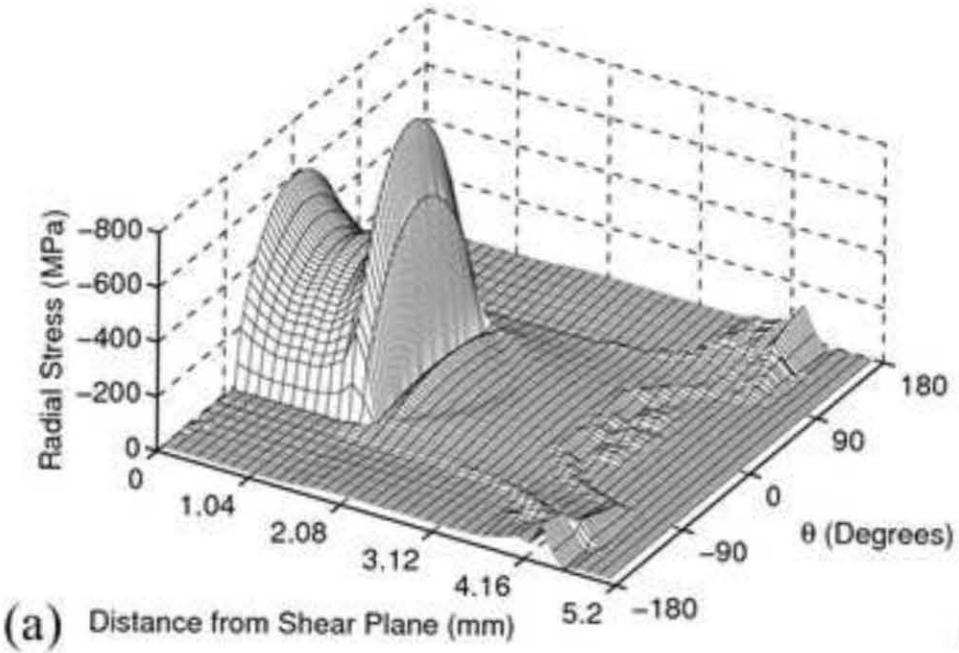

(a)

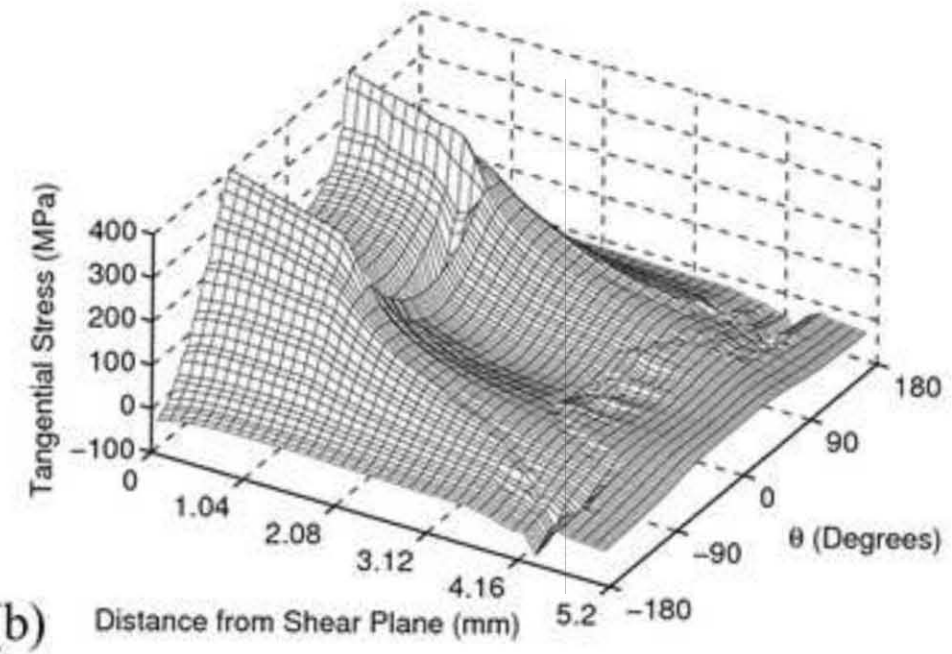

(b)

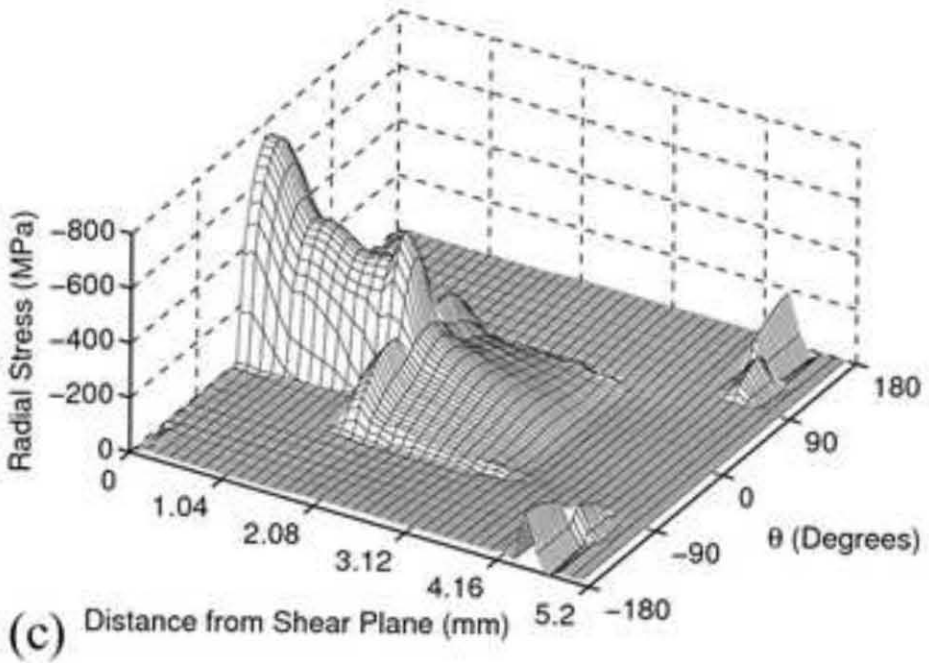

(c)

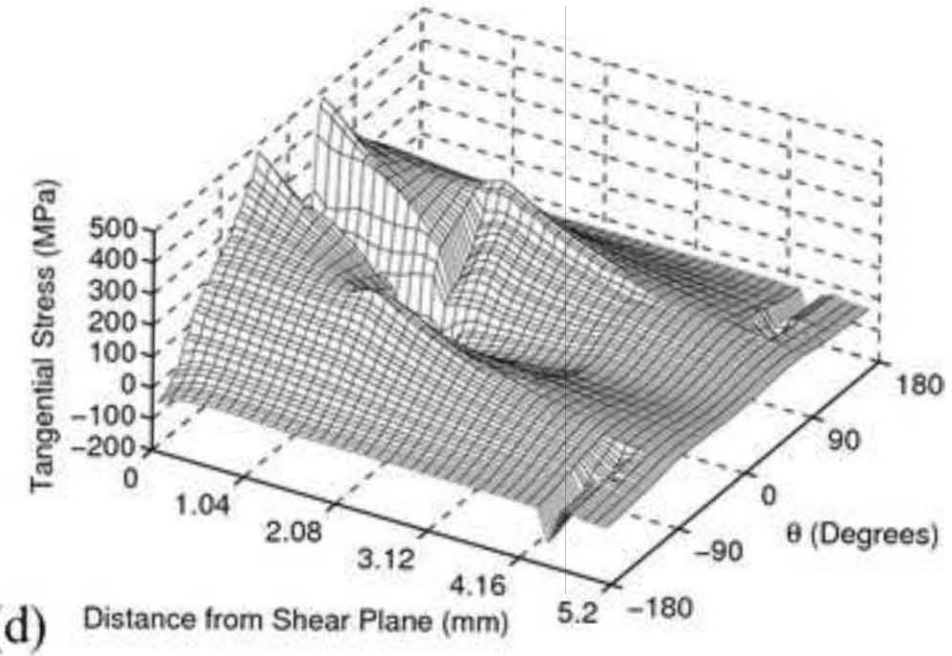

(d)

Figure14

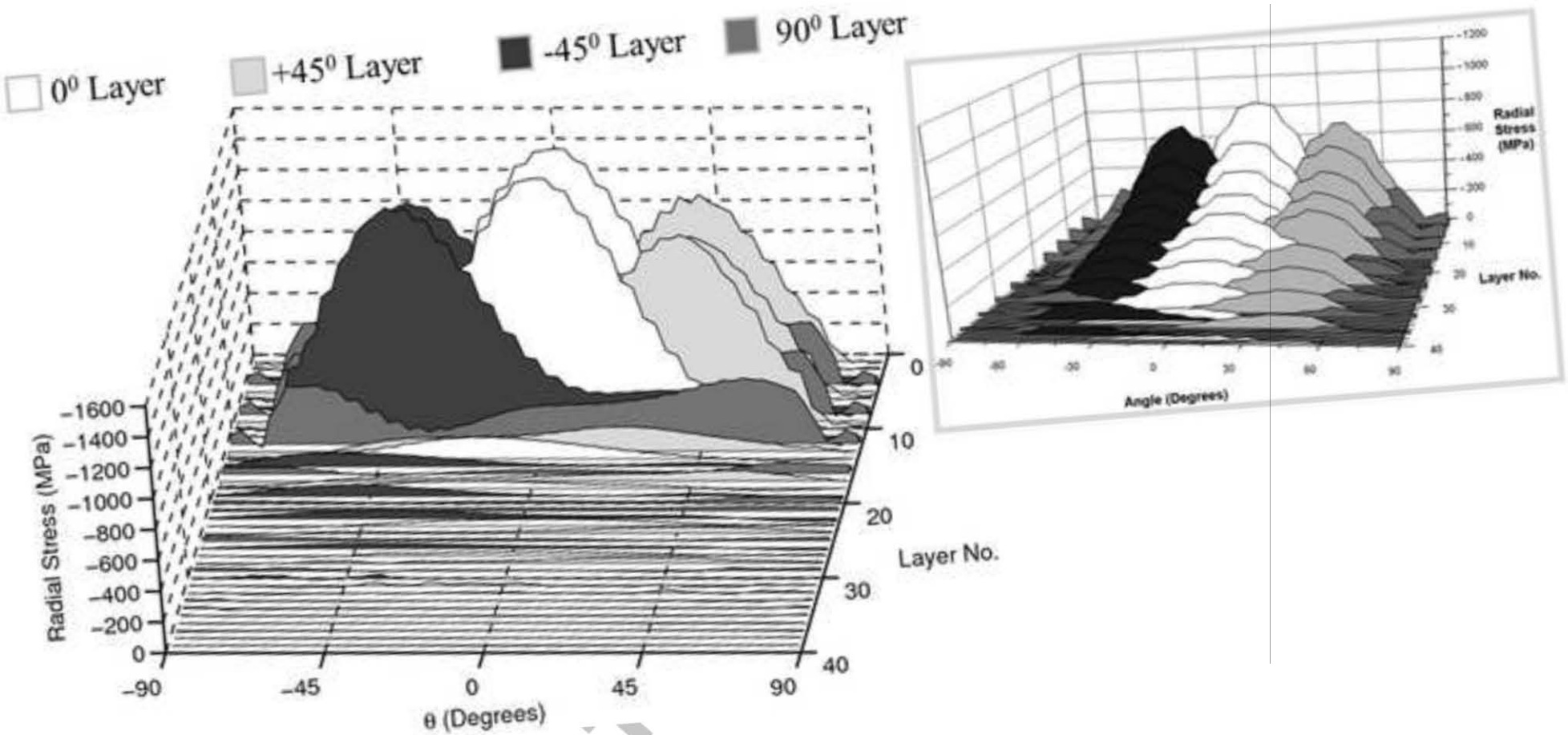

Figure15

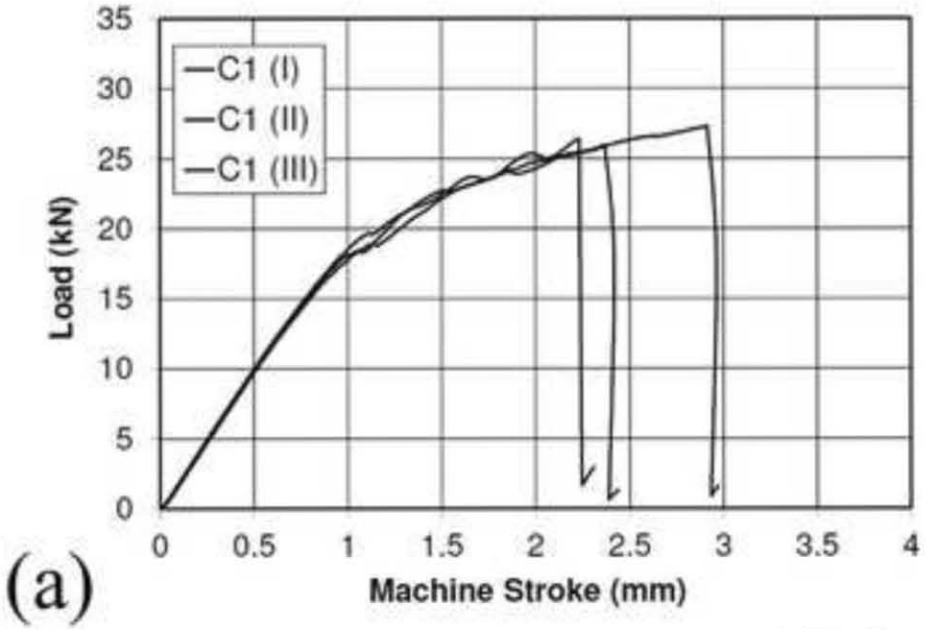

(a)

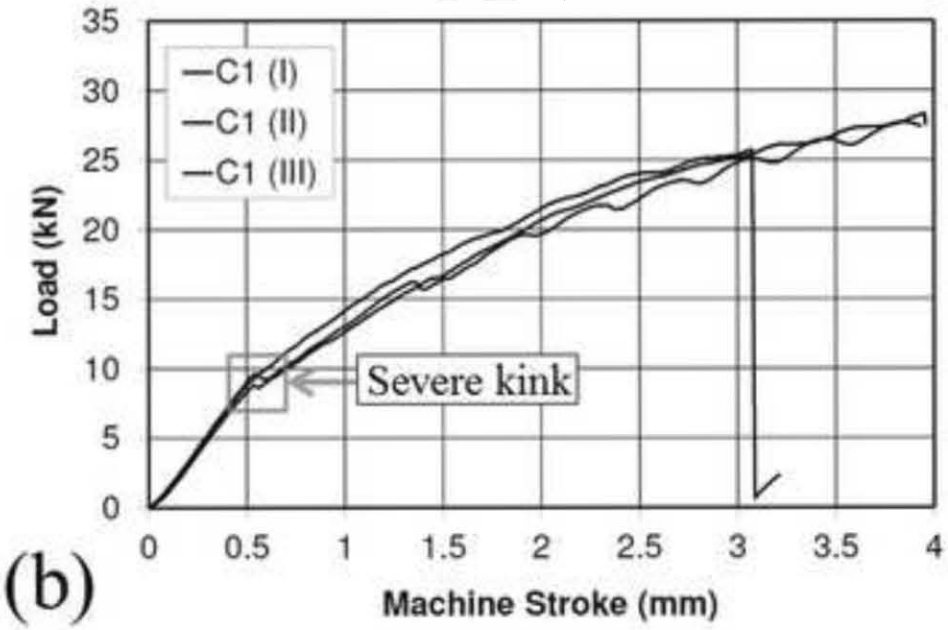

(b)

Figure16

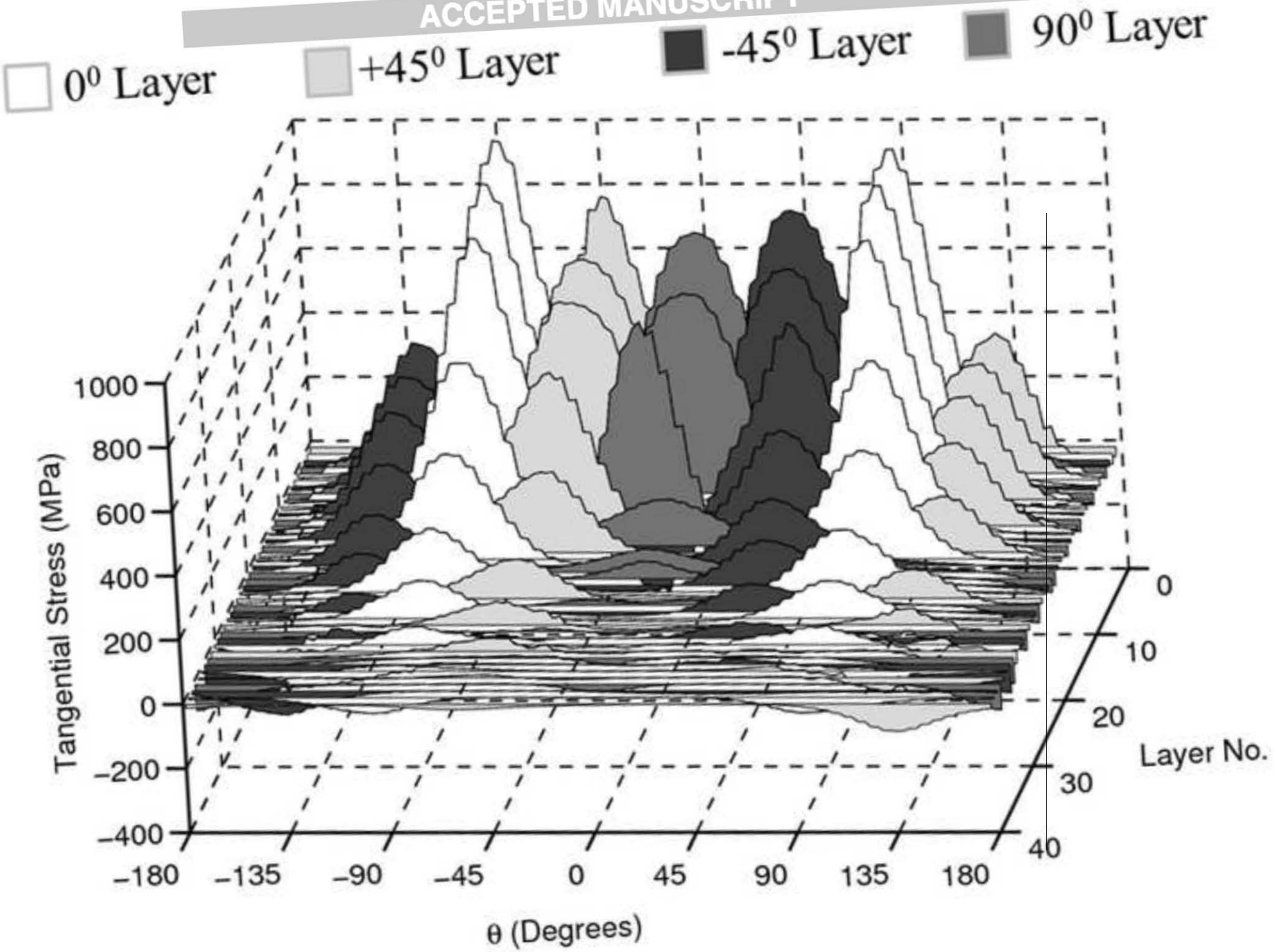

Figure17

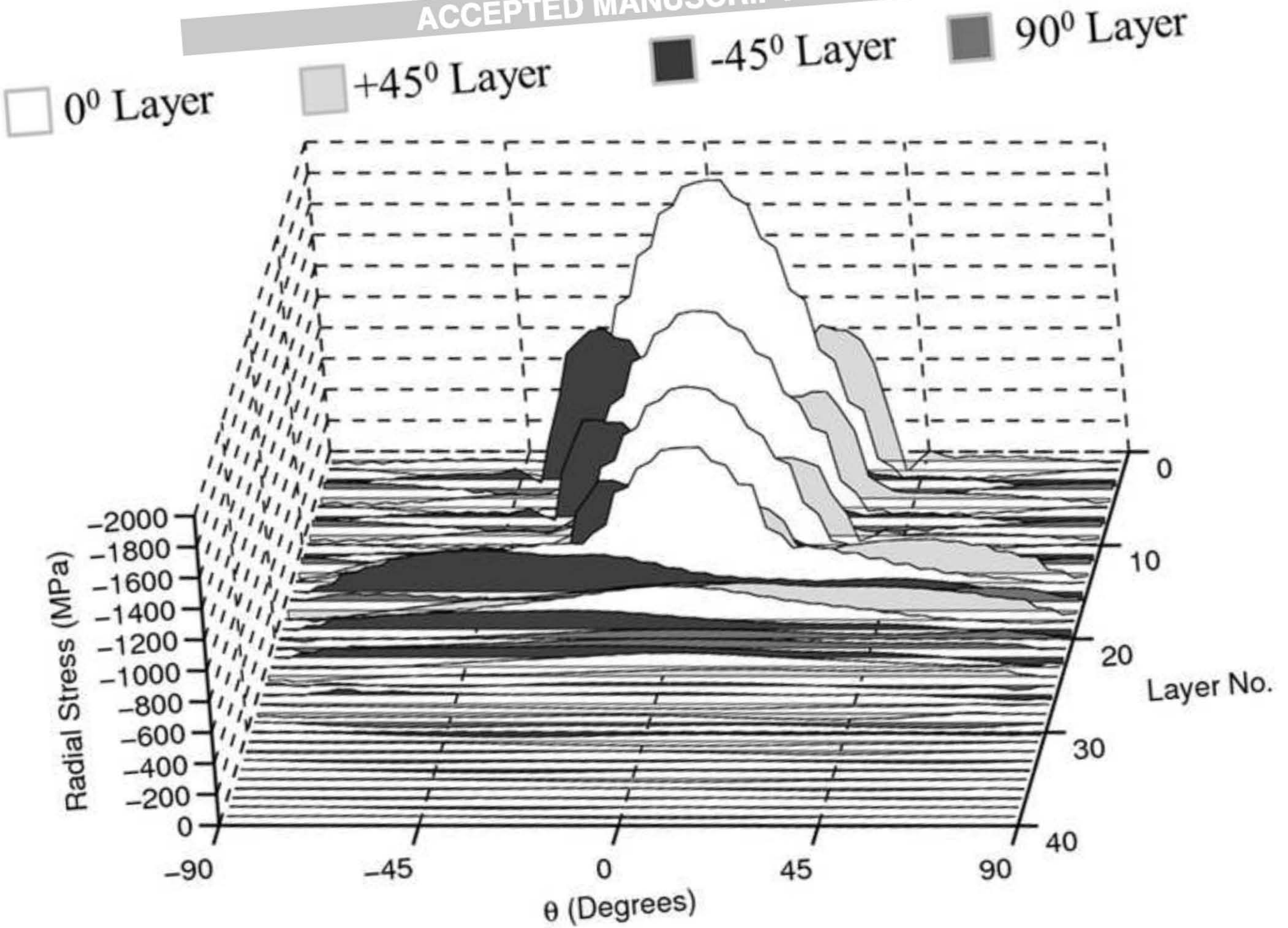

Figure18

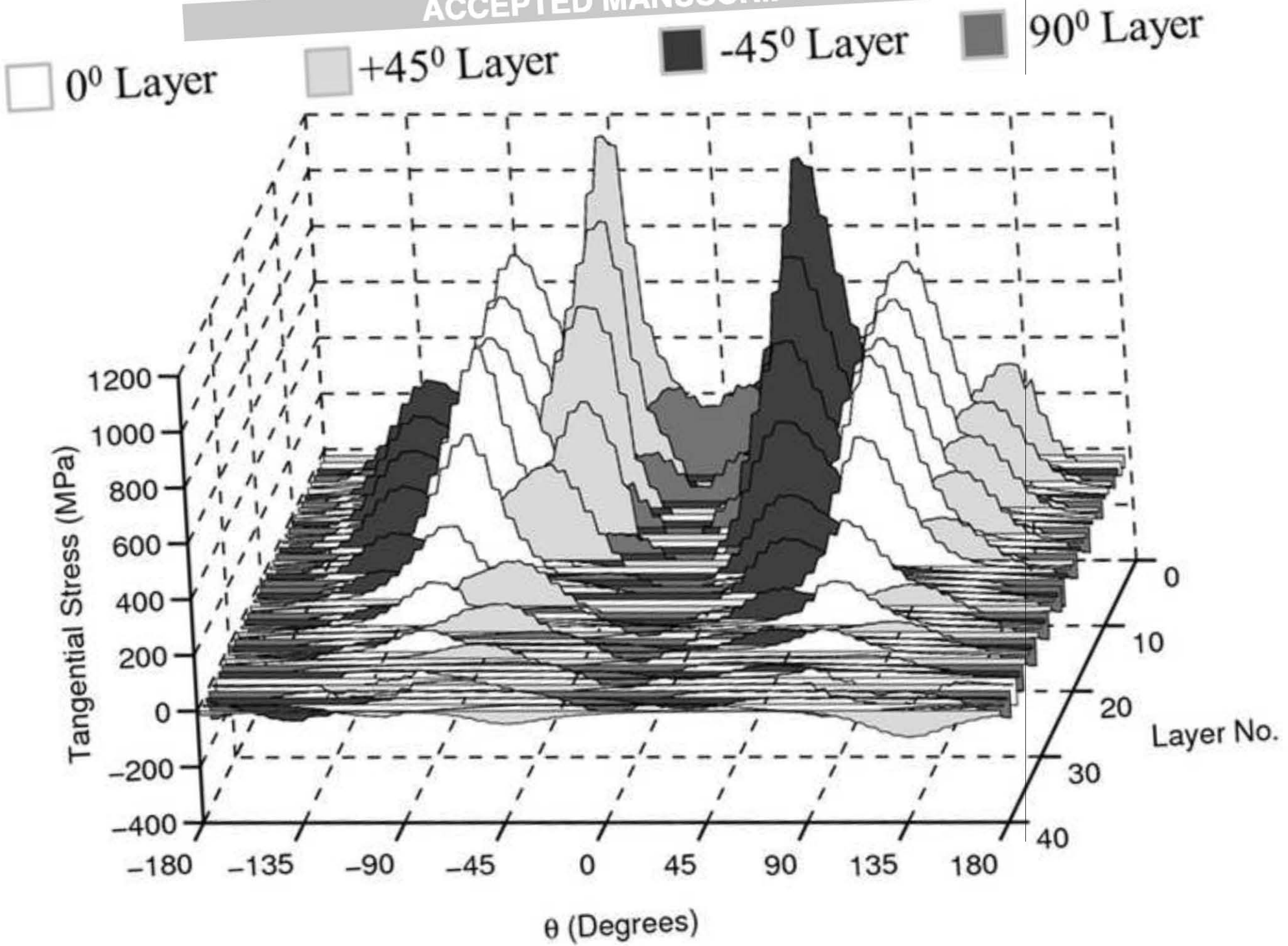

Figure19

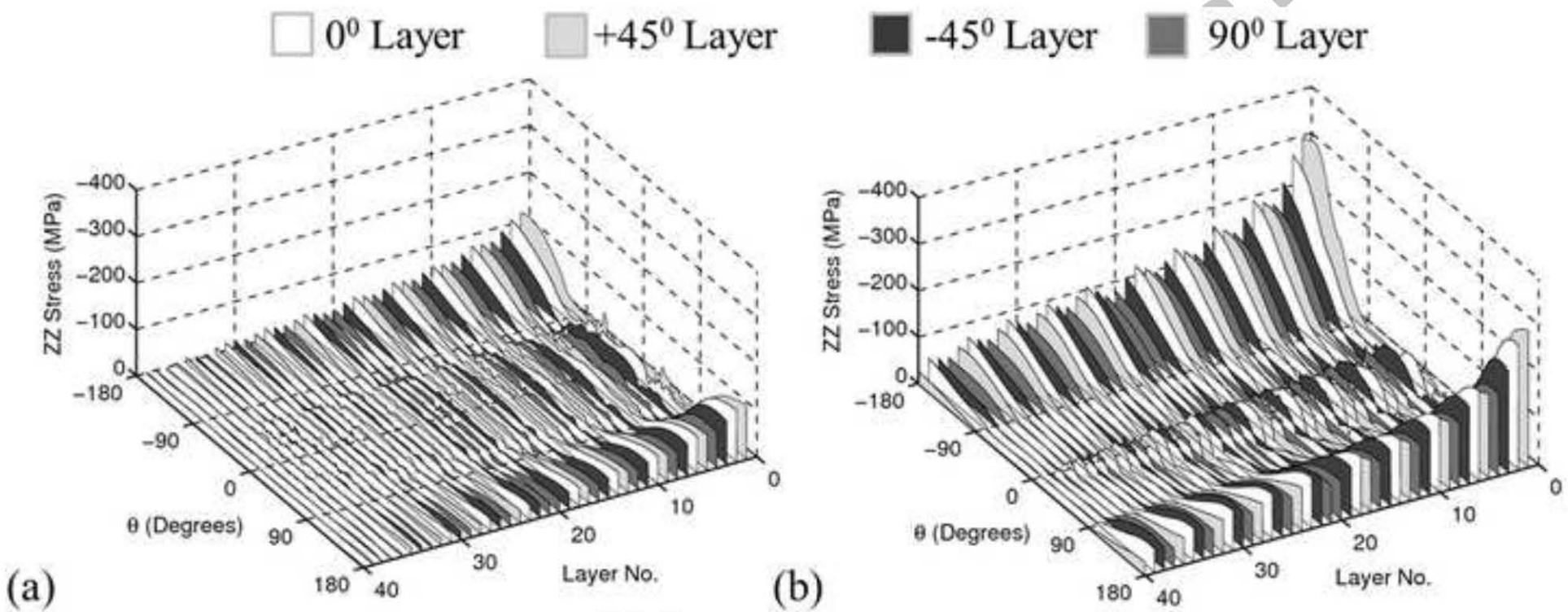

Figure20

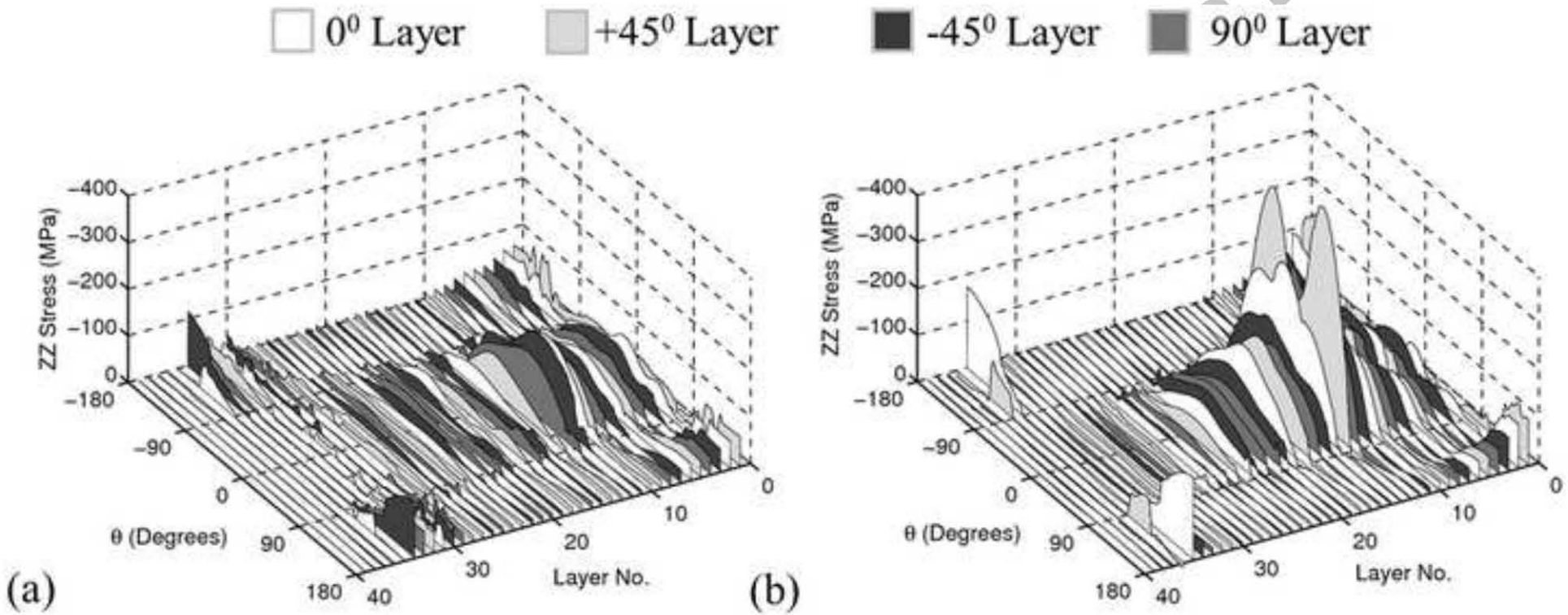

Figure21